Recently, we reported the novel *ALS2* homologous gene, ALS2 C-terminal like (*ALS2CL*) and its murine ortholog (*Als2cl*) [14]. The *ALS2CL* gene encodes a 108 kDa protein, ALS2CL, comprising several domains and motifs including MORN and VPS9. ALS2CL exhibits rather strong Rab5-binding properties but a relatively weak Rab5GEF activity [14]. Co-expression of ALS2CL and Rab5 results in a unique tubulation phenotype of endosome compartments with significant colocalization of ALS2CL and Rab5 in HeLa cells. Thus, ALS2CL and ALS2 play overlapping but distinctive roles on the Rab5-mediated membrane dynamics in the cells, tempting to speculate that ALS2CL modulates the ALS2-mediated molecular and cellular functions.

In the present study, we investigated the molecular features of ALS2CL and its functional relationship with ALS2. Our studies reveal that ALS2CL is a novel ALS2-binding protein and modulates ALS2-mediated membrane dynamics. Thus, ALS2CL might act as a modulator in the ALS2- and Rab5-mediated membrane trafficking *in vivo*.

Materials and methods

Antibodies. Anti-ALS2CL rabbit polyclonal antibody (pAb) (CLHPF560–953) was raised by immunizing Japanese White rabbit with the recombinant peptide of human ALS2CL spanning 560–953 amino acids (aa), followed by affinity-purification using an antigen coupled sepharose column. Other antibodies used in this study are listed in Supplementary Materials and Methods.

Plasmid constructs. All cDNA clones used in this study were obtained by subcloning the PCR or the reverse transcriptase-PCR-amplified fragments into the appropriate expression vectors as described [8,14,15]. The DNA sequence of the insert as well as its flanking regions in each plasmid construct was verified by sequencing. For the antibody generation, the cDNA fragment of human *ALS2CL*, encoding the region spanning 560–953aa, was subcloned into pRSET Bacterial Expression Vector (Invitrogen), generating pRSETHis-hALS2CL_560–953. For the co-immunoprecipitation, gel filtration, and subcellular localization studies, the cDNA fragments of human *ALS2CL*, mouse *Als2cl*, and mouse *Als2* were subcloned into the modified pCI-neo Mammalian Expression Vector (Promega), allowing the production of the N-terminally FLAG- or HA-tagged human ALS2CL (hALS2CL), mouse ALS2 (mALS2), and mouse ALS2CL (mALS2CL) proteins, and their deletion mutants. Previously generated pEGFP-hALS2_L [8], and pEGFP-hASLS2_695–1657 [9] were also utilized.

Cell culture, transfection, and Western blot analysis. Details of these methods are available in Supplementary Materials and Methods.

Co-immunoprecipitation, gel filtration, and immunocytochemistry. Co-immunoprecipitation assay, gel filtration and immunofluorescence studies were conducted as previously described [8,9,15]. Details of these methods are available in Supplementary Materials and Methods.

Preparation of the ALS2/ALS2CL complex. COS-7 cells that were transfected with pCIneoFLAG-mALS2_1012–1651 or pCIneoHA-mALS2CL were lysed in buffer A consisting of 50 mM Tris–HCl (pH 7.5), 150 mM NaCl, 1 mM EDTA, 2% Tween 20, and Complete protease inhibitor mixture (Roche) and immunoprecipitated using EZview™ Red ANTI-FLAG M2 or ANTI-HA affinity gel (Sigma). These affinity gels conjugating ALS2 or ALS2CL were washed three times with the ice-cold buffer B consisting of 50 mM Tris–HCl (pH 7.5), 150 mM NaCl, and 1% Tween 20. The N-terminally FLAG-tagged mALS2_1012–1651 protein on the ANTI-FLAG affinity gels were eluted with buffer B containing 500 μg/ml 3× FLAG peptide (Sigma) for 1 h at 4 °C. The eluted sample was mixed with the ANTI-HA affinity gel conjugated with N-terminally HA-tagged mouse ALS2CL, and incubated for 2 h at 30 °C. The affinity gels were washed three times with appropriate buffer, and subjected to gel filtration.

Results

Interaction of ALS2CL with ALS2

We have previously demonstrated that ALS2 forms a homophilic oligomer through its distinct C-terminal regions [9]. Further, analysis of the predicted amino acid sequences revealed a high level of sequence similarity throughout the entire region of ALS2CL and the C-terminal half of ALS2 [14], tempting to speculate that ALS2CL can interacts itself and also interacts with ALS2. To confirm these possibilities, we generated various truncated ALS2CL-expressing constructs and used them in the Y2H tests (Fig. S1). As we expected, ALS2CL could self-associate, and two distinct regions of ALS2CL, 329–582aa and 652–953aa, are indispensable for its self-interaction in yeast cells, consistent with the previous finding that ALS2 can self-interact in a similar manner [9]. We also demonstrated that ALS2CL could interact with ALS2 by the Y2H assays. Interestingly, ALS2CL interacted with ALS2 through the regions between the central region (329–651aa) of ALS2CL and the C-terminal VPS9-containing region (1351–1657aa) of ALS2, but not the regions between the ALS2CL C-terminus VPS9-containing region and the ALS2 MORN-containing region in yeast (Fig. S1).

To confirm this interaction, we transfected the expression constructs of human ALS2 (pCIneo-FLAG_hALS2_L) along with human ALS2CL (pCIneoHA_hALS2CL) into COS-7 cells and performed co-immunoprecipitation using the ANTI-FLAG affinity gel. HA-tagged hALS2CL was efficiently co-immunoprecipitated with FLAG-tagged hALS2_L (Fig. 1A). HA-tagged hALS2_L was also co-immunoprecipitated with FLAG-tagged hALS2CL (Fig. 1B, lane 2). We also obtained similar results using mouse ALS2CL and ALS2 (Fig. S2). Next, to confirm the responsible regions for the interaction, we generated the expression constructs encoding various FLAG-tagged deletion mutants of ALS2CL. HA-tagged hALS2_L was co-immunoprecipitated with FLAG-tagged hALS2CL_329–953 (Fig. 1B, lane 8), but not with FLAG-tagged hALS2CL_1–582 (Fig. 1B, lane 5) or FLAG-tagged hALS2CL_560–953 (Fig. 1B, lane 11). These results indicate that ALS2CL, through the region of 329–953aa, interacts with ALS2 in mammalian cells. In addition, endogenous ALS2, albeit rather lower level, was also detected in the FLAG-immunoprecipitated pellets prepared from COS-7 cells singly overexpressing FLAG_hALS2CL using anti-ALS2 pAb (HPF1–680) (data not shown), supporting the molecular interaction between ALS2CL and ALS2 in the cells.

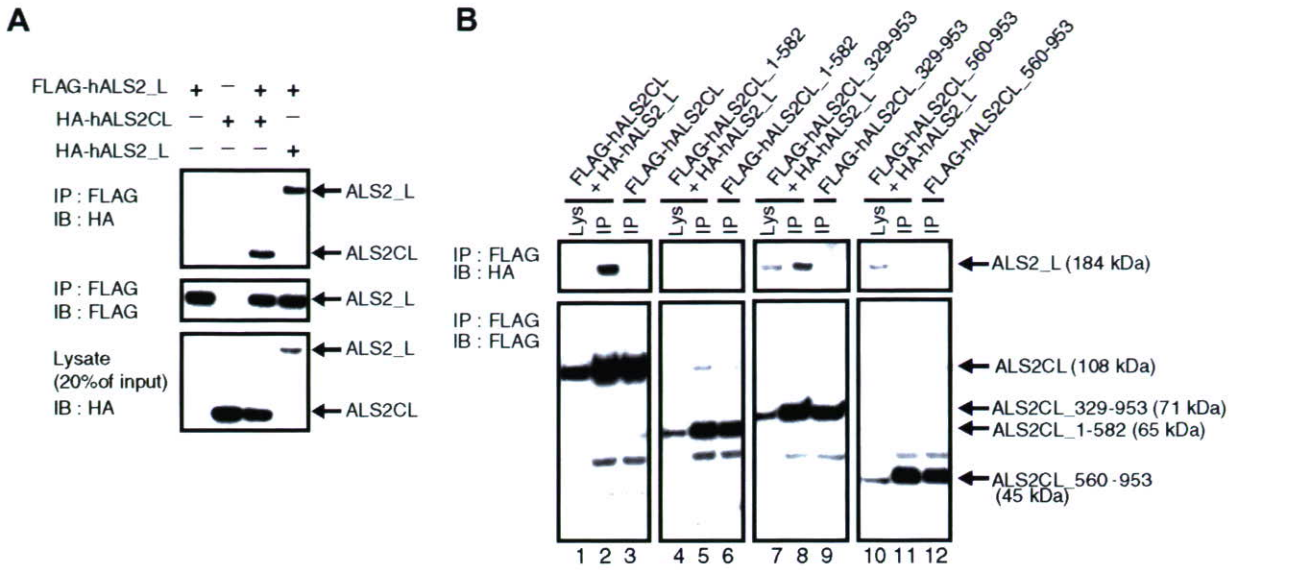

Fig. 1. Co-immunoprecipitation of ALS2CL and ALS2. (A) Western blot analyses of immunoprecipitates (top and middle) and lysates (20% of input) (bottom) derived from COS-7 cells overexpressing either human ALS2 or human ALS2CL, or combinations as indicated. ALS2 self-interaction [9] was used as a positive control. (B) Mapping of the ALS2-interacting domains of ALS2CL. Western blot analyses of lysates (*Lys*) (14% of input) and immunoprecipitates (IP) derived from COS-7 cells that were transfected with expression constructs as follows, double transfection; pCIneoFLAG-hALS2CL and pCIneoHA-hALS2_L (lanes 1 and 2), pCIneoFLAG-hALS2CL_1–582 and pCIneoHA-hALS2_L (lanes 4 and 5), pCIneoFLAG-hALS2CL_329–953 and pCIneoHA-hALS2_L (lanes 7 and 8), and pCIneoFLAG-hALS2CL_560–953 and pCIneoHA-hALS2_L (lanes 10 and 11), single transfection; pCIneoFLAG-hALS2CL (lane 3), pCIneoFLAG-hALS2CL_1–582 (lane 6), pCIneoFLAG-hALS2CL_329–953 (lane 9), and pCIneoFLAG-hALS2CL_560–953 (lane 12). IP, antibody used for immunoprecipitation; IB, antibody used for Western blot analysis.

Hetero-oligomerization of the ALS2CL and ALS2 proteins

Previously, we have demonstrated that ALS2 forms a very stable homophilic oligomer through the C-terminal MORN/VPS9 region in a native state, and this homo-oligomerization is crucial for the Rab5GEF activity [9]. To characterize the oligomerization for ALS2CL, we conducted a gel filtration analysis. HA-tagged mALS2CL was affinity-purified from the extract of transfected COS-7 cells, and separated by the gel filtration column. Elute was analyzed by Western blot analysis using anti-ALS2CL pAb (CLHPF560–953). HA-tagged mALS2CL (~108 kDa in SDS–PAGE) was eluted in fractions with an apparent peak molecular mass of ~220 kDa (Fig. 2A). It is noteworthy that no ALS2CL molecule was found in the fractions corresponding to a monomeric form (~108 kDa). Because no other proteins co-purified with HA-tagged ALS2CL were observed in Coomassie brilliant blue staining of the SDS–PAGE gels (data not shown), a majority of the ALS2CL molecules is likely to be present as a dimeric form in a native state.

To investigate whether dimerized ALS2CL molecules directly interact with oligomerized ALS2, mixtures of purified HA-tagged mALS2CL and FLAG-tagged mALS2_1012–1651 (spanning the MORN/VPS9 region; a minimum oligomerization-prone and Rab5GEF-mediated fragment) were subjected to the gel filtration analysis. Both HA-tagged mALS2CL (108 kDa) and FLAG-tagged mALS2_1012–1651 (75 kDa) were eluted in fractions representing up to an apparent molecular mass of ~1000 kDa (Fig. 2C), which was significantly higher than the peak molecular mass for the homophilic form of either the ALS2 fragment (~600 kDa) (Fig. 2B) or ALS2CL (Fig. 2A), although HA-tagged mALS2CL was also detected in rather broad range of fractions (200–1000 kDa). The enrichment of ALS2/ALS2CL complexes in the ~1000 kDa faction was confirmed by densitometric analysis (Fig. 2D). These results indicate that ALS2CL and ALS2_1012–1651 could form a large heteromeric complex in a native state when co-existed.

To examine the effect of ALS2CL on ALS2-associated Rab5GEF activity, a sample of the ALS2/ALS2CL complexes with an excess amount of ALS2CL was subjected to the *in vitro* GDP dissociation assay on Rab5A. Notably, addition of an excess amount of ALS2CL to ALS2_1012–1651 revealed the additive Rab5GEF activity rather inhibitory or stimulatory (Fig. S3). The results imply that the interaction of ALS2CL with ALS2 and/or the presence of excess ALS2CL do not crucially affect the ALS2-mediated Rab5GEF activity *in vitro*.

Effect of ALS2CL expression on subcellular localization of ALS2

Previously, we reported that ectopically expressed ALS2_L mostly distributed in cytoplasm in a diffused manner (Fig. 3A) [8], while ectopically expressed ALS2CL was localized throughout the cells with strong punctuated stainings in cytoplasm (Fig. 3B) [14]. To investigate the effect of ALS2CL expression on the subcellular localization of

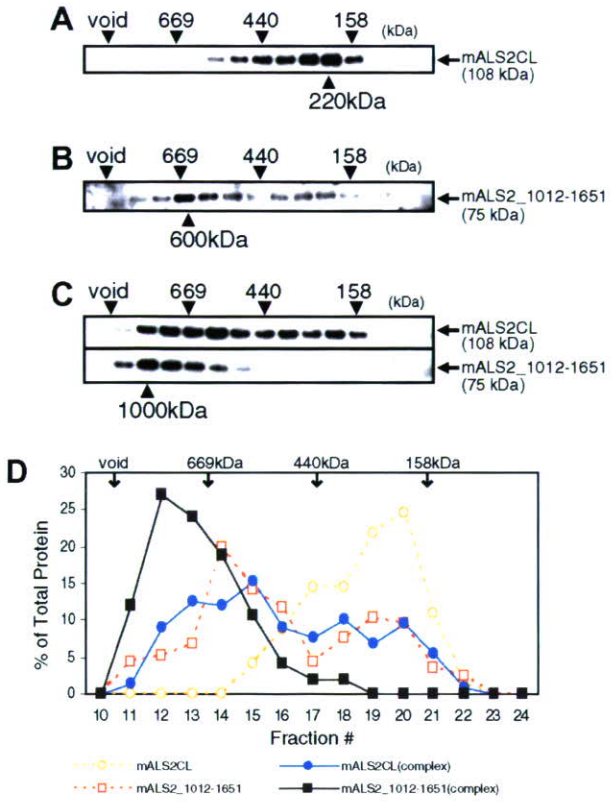

Fig. 2. Gel filtration analysis of ALS2CL and the ALS2/ALS2CL heteromeric complex. (A) Western blot analysis of the gel-fractionated HA-tagged mALS2CL. HA-tagged mALS2CL was purified from COS-7 cells transfected with pCIneoHA-mALS2CL, and applied to a Superdex 200 gel filtration column. The fractions were analyzed by Western blot analysis with the anti-ALS2CL pAb (CLHPF560–953). Molecular masses of the sizing standards are shown on the top. Elution peak for HA-tagged mALS2CL (~220 kDa) is indicated by the arrowhead. (B) Western blot analysis of the gel-fractionated FLAG-tagged mALS2_1012–1651. Gel filtration was performed as in (A). The fractions were analyzed by Western blot analysis with the anti-ALS2 pAb (MPF1012–1651). Molecular size of the elution peak for FLAG-tagged mALS2_1012–1651 is ~600 kDa as indicated by the arrowhead. (C) Western blot analysis of the gel-fractionated ALS2/ALS2CL complex. Gel filtration was performed as in (A). The fractions were analyzed by Western blot analysis with the anti-ALS2CL pAb (CLHPF560–953) and anti-ALS2 pAb (MPF1012–1651). Molecular size of the elution peak for ALS2/ALS2CL complex is ~1000 kDa as indicated by the arrowhead. (D) Densitometric analysis of the fractionated HA-tagged mALS2CL, FLAG-tagged mALS2_1012–1651, and ALS2/ALS2CL complex. Each fraction was expressed as a percentage of the total protein across the entire fractions.

ALS2, HeLa cells were co-transfected with the constructs expressing FLAG-tagged hALS2CL and EGFP-fused hALS2_L, and analyzed immunocytochemically. Interestingly, both proteins were significantly co-distributed onto the vesicular compartments in cytoplasm, when FLAG-tagged hALS2CL and EGFP-fused hALS2_L were co-expressed (Fig. 3C). A similar result was obtained with the use of constructs expressing mouse counterparts (data not shown). These results suggest that co-expression of ALS2CL with ALS2 facilitates membrane distribution of ALS2 in the cells.

To confirm whether the ALS2CL affects intracellular distribution of ALS2, COS-7 cells transfected with the constructs expressing either human ALS2CL (FLAG-tagged hALS2CL) or human full length ALS2 (HA-tagged hALS2_L), or both, were lysed and separated into detergent-soluble and -insoluble fractions. HA-tagged hALS2_L abounded in detergent soluble fractions (Fig. 3D, lanes 1 and 2), while a majority of FLAG-tagged hALS2CL was present in detergent insoluble fractions (Fig. 3D, lanes 3 and 4). Co-expression of hALS2_L and hALS2CL resulted in a significant increase in the detergent insoluble form of ALS2 without changing the distribution of ALS2CL (Fig. 3D, lanes 7 and 8). Importantly, FLAG-tagged hALS2CL_560-953, lacking the interacting domain with ALS2 (Fig. 1B), showed no observable effects on the ALS2 distribution (Fig. 3D, lanes 9 and 10). Thus, these results indicate that the intracellular localization of ALS2 can be altered by the interaction with ALS2CL.

Effect of ALS2CL on the ALS2-mediated endosomal dynamics

To investigate whether ALS2CL affects the ALS2 function in the cells, HeLa cells were co-transfected with the constructs expressing FLAG-tagged hALS2CL and EGFP-fused hALS2_695–1657, and subjected to the fluorescence microscopic observations. As previously reported [8,9], expression of a constitutively active form of human ALS2, EGFP-fused hALS2_660–1657 [8] or EGFP-fused hALS2_695–1657 [9], caused the endosome enlargement via the endogenous Rab5 activation (Fig. 4A). When FLAG-tagged hALS2CL was co-expressed with EGFP-fused hALS2_695–1657, enlarged endosome phenotypes were dominantly suppressed, and instead striking tubular membranous structures in the perinuclear area, which accompanied an extensive co-localization of hALS2CL and hALS2_695–1657, resulted (~15% of the co-transfected cells) (Fig. 4B, upper panel). Importantly, FLAG-tagged hALS2CL_560–963, lacking the interacting domain with ALS2 (Fig. 1B), showed no observable effects on the ALS2-mediated endosome enlargement (Fig. 4B, lower panel). These data strongly suggest that ALS2CL can modulate the ALS2-mediated endosome dynamics through their molecular interaction in the cells. Further, a series of double staining experiments revealed that the tubular structures were significantly overlapped with microtubules (Fig. 4C), but rarely with either F-actin, early endosome associated protein EEA1, recycling endosome marker transferrin receptor, or Golgi marker GM130 (data not shown).

Discussion

In this study, we reported that ALS2CL directly interacted with ALS2 and altered the ALS2-mediated enlarged endosome phenotypes. Our results implicate that ALS2CL is a novel ALS2-interactor modulating the ALS2-mediated membrane dynamics in the cells.

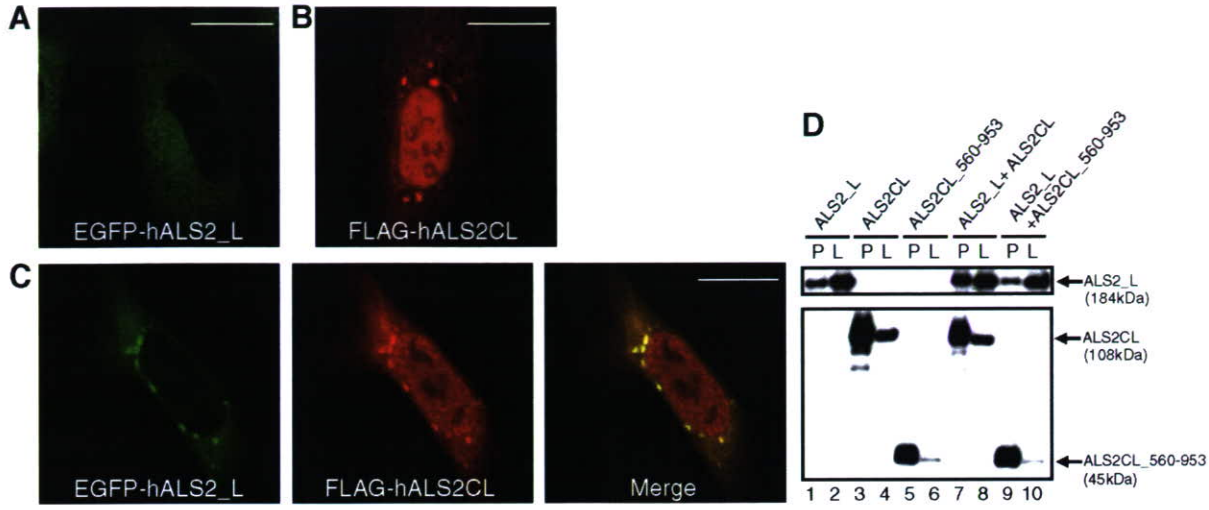

Fig. 3. Effect of ALS2CL overexpression on the subcellular localization of ALS2. (A) Subcellular distribution of the ectopically expressed EGFP-fused hALS2_L in HeLa cells. (B) Subcellular distribution of the ectopically expressed FLAG-tagged hALS2CL in HeLa cells. (C) Co-transfection of the EGFP-fused hALS2_L and FLAG-tagged hALS2CL in HeLa cells (pCIneoEGFP-hALS2_L; pCIneoFLAG-hALS2CL = 7:3). Scale bars, 20 μm. (D) Western blot analyses of pellets and lysates derived from COS-7 cells that were co-transfected with two selected expression plasmids with a combination of pCIneoHA-hALS2_L and pCIneo-empty (lanes 1 and 2), pCIneoFLAG-hALS2CL and pCIneo-empty (lanes 3 and 4), pCIneoFLAG-hALS2CL_560–953 and pCIneo-empty (lanes 5 and 6), pCIneoHA-hALS2_L and pCIneoFLAG-hALS2CL (lanes 7 and 8), or pCIneoHA-hALS2_L and pCIneoFLAG-hALS2CL_560–953 (lanes 9 and 10). The fractions were analyzed by Western blot analysis with the anti-ALS2 pAb (HPF1–680) and the anti-ALS2CL pAb (CLHPF560–953). P, pellet (detergent insoluble fraction); L, lysate (detergent soluble fraction).

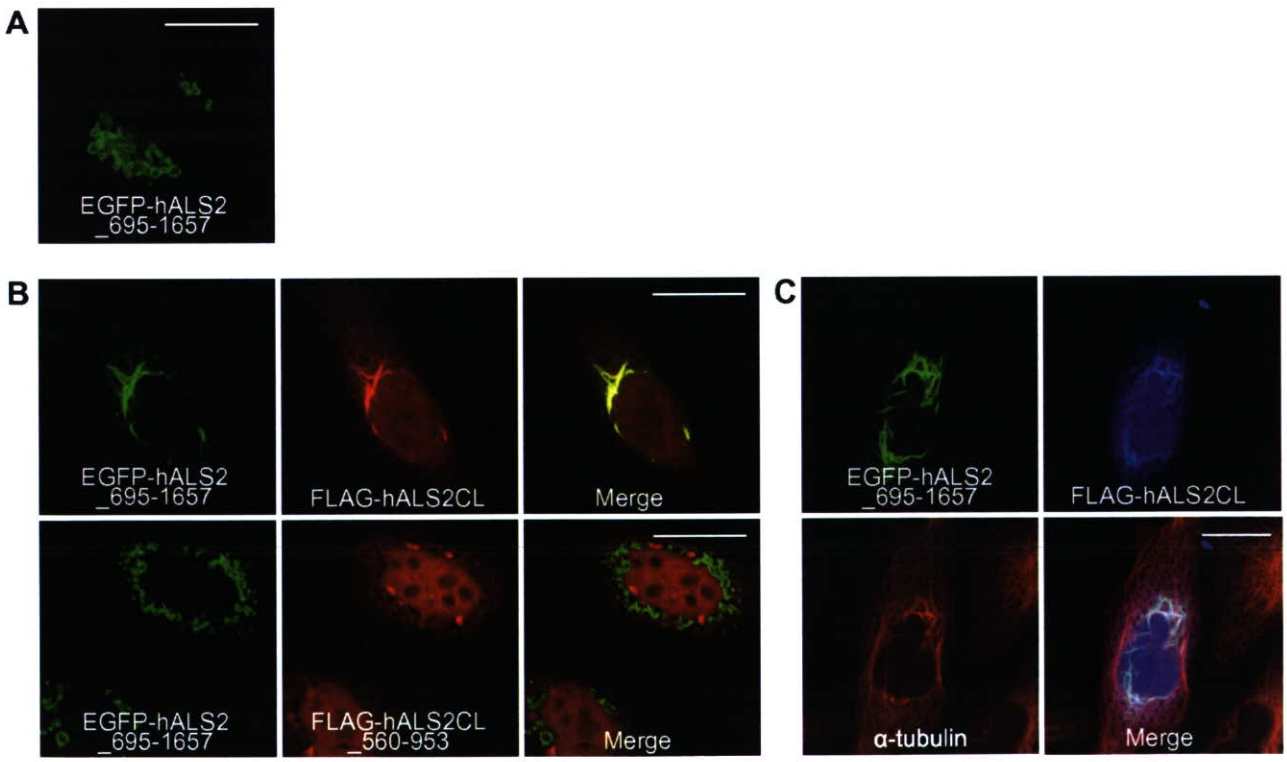

Fig. 4. Effects of ALS2CL overexpression on the ALS2-mediated endosome dynamics in HeLa cells. (A) Subcellular distribution of the ectopically expressed EGFP-fused hALS2_695–1657 in the cells. (B) Co-transfection of the EGFP-fused hALS2_695–1657 and FLAG-tagged hALS2CL in the cells (pCIneoEGFP-hALS2_695–1657; pCIneoFLAG-hALS2CL = 1:1) (upper panel). Co-transfection of the EGFP-fused hALS2_695–1657 and FLAG-tagged hALS2CL_560–953 in the cells (pCIneoEGFP-hALS2_695–1657; pCIneoFLAG-hALS2CL_560–953 = 1:1) (lower panel). (C) Tubular structures were distributed along endogenous microtubules stained with anti-α tubulin monoclonal antibody (mAb). Co-transfection was performed as in (B). Scale bars, 20 μm.

Recently, we have demonstrated that ALS2 molecules form a homophilic oligomer through its distinct C-terminal regions [9]. Because the entire region of ALS2CL is highly homologous to the C-terminal half of ALS2 [14], we predicted that ALS2CL molecules also formed a homophilic oligomer. As expected, Y2H experiment found that ALS2CL molecules could self-interact through its distinct regions, whose manner was analogous to the ALS2 self-interaction. However, a series of our gel filtration analyses revealed that a majority of ALS2CL molecules was present as a dimeric form, while ALS2 existed as a homo-oligomer [9]. Here we also demonstrated that ALS2CL directly interacted with ALS2. Y2H showed that the region spanning 329–651aa of ALS2CL interacted with the C-terminal 1351–1657aa region of ALS2, while the C-terminal region of ALS2CL (652–953aa) failed to interact with the ALS2 1041–1351aa fragment, consistent with co-immunoprecipitation experiment. This indicates that the interaction between ALS2CL and ALS2 is achieved through distinct regions from those requisite for the ALS2CL or ALS2 self-interaction. Further, gel filtration analyses revealed that molecular size of the distribution of ALS2CL and ALS2 molecules, when co-existed, was much larger than that of either ALS2CL homo-dimer or ALS2 homo-oligomer. Moreover, we showed that such ALS2/ALS2CL complex still retained the Rab5GEF activity *in vitro*. Taken together, these results suggest that, at least *in vitro*, ALS2CL and ALS2 molecules form themselves into a large heteromeric protein complex, consisting of ALS2CL dimer and ALS2 oligomer, which is an enzymatically active Rab5GEF molecule. Since endogenous ALS2 in COS-7 cells can interact with overexpressed ALS2CL (data not shown), we suspected the interaction between endogenous ALS2CL and ALS2. However, further detailed studies will be required to reach the conclusion.

Most remarkable finding in this study was that co-expression of ALS2CL and ALS2_695–1657 resulted in a complete loss of enlarged endosomal phenotypes and instead prominent tubular/elongated membranous structures appeared in the perinuclear cytoplasm, which were dependent upon the ALS2CL–ALS2 interaction. Previously, we have demonstrated that the C-terminal ALS2 peptide containing 660–1657aa or 695–1657aa induces the enlargement of endosomes via the activation of endogenous Rab5, and that co-expression of hALS2_660–1657 and Rab5A reveals a further enlargement of endosomes [8,9]. Thus, the ALS2 peptide spanning the DH/PH/MORN/VPS9 domains with devoid of the N-terminal RLD region acts as a constitutively active Rab5GEF form of ALS2 in the cells [8]. Despite the fact that ALS2CL shares a significant homology to this active fragment of ALS2, co-expression of ALS2CL and Rab5 does not induce the enlargement of endosomes but rather results in a unique tubulation phenotype of endosome compartments with significant co-localization of ALS2CL and Rab5 [14]. We here showed that ALS2CL altered full length of ALS2 localization in the cells, but did not affect the ALS2-mediated Rab5GEF activity *in vitro*. These data suggest that ALS2CL can modulate ALS2- and Rab5-mediated endosome dynamics by altering intracellular ALS2 distribution and thus the intrinsic ALS2 function *in situ*. Further, we identified that the tubular structures, which were induced by the co-expression of ALS2CL and ALS2_695–1657, significantly overlapped with microtubules. Because Rab5 plays a crucial role in regulating endosome motility along microtubules [16], it is conceivable that ALS2CL modulates not only ALS2- and Rab5-regulated membrane fusion but also microtubule-mediated membrane/vesicle trafficking via the ALS2CL–ALS2 interaction in the cells. To clarify the molecular mechanisms underlying such cellular processes regulated by ALS2 and ALS2CL *in vivo*, further studies will be required.

We have previously proposed that a perturbation of endosome dynamics caused by loss of ALS2-associated Rab5GEF activity might underlie neuronal dysfunction and degeneration in the ALS2-linked MNDs [8]. In addition, several causative genes underlying MNDs, whose gene products are involved in intracellular vesicle/membrane trafficking, have recently been identified [17]. Further dissection of molecular and cellular functions of such associated or related factors including ALS2CL will give us important insights into the pathogenesis for the ALS2-linked MNDs.

Acknowledgments

We thank Mses. Junko Showguchi-Miyata, Yoshiko Yanagisawa, and Etsuko Suga for their technical assistance, and all the members of our laboratory for helpful discussion and suggestions. This work was funded by the Japan Science and Technology Agency (to J.E.I.), the Ministry of Health, Labour and Welfare (to J.E.I.). S.H. receives support for a Grant-in-Aid for Scientific Research from JSPS, Grant-in-Aid for Scientific Research on Priority Areas—Research on Pathomechanisms of Brain Disorders—from MEXT, Takeda Science Foundation, the Sumitomo Foundation, the Naito Foundation, NOVARTIS Foundation (Japan) for the Promotion of Science, and The Ichiro Kanehara Foundation, K.S.-U. and R.K. are supported by a 2006 Tokai University School of Medicine Research Aid, and A.O. is supported by a Research Fellowship for Young Scientist from JSPS.

Appendix A. Supplementary data

Supplementary data associated with this article can be found, in the online version, at doi:10.1016/j.bbrc.2006.12.229.

References

[1] S. Hadano, C.K. Hand, H. Osuga, Y. Yanagisawa, A. Otomo, R.S. Devon, N. Miyamoto, J. Showguchi-Miyata, Y. Okada, R. Singaraja, D.A. Figlewicz, T. Kwiatkowski, B.A. Hosler, T. Sagie,

J. Skaug, J. Nasir, R.H. Brown Jr., S.W. Scherer, G.A. Rouleau, M.R. Hayden, J.-E. Ikeda, A gene encoding a putative GTPase regulator is mutated in familial amyotrophic lateral sclerosis 2, Nat. Genet. 29 (2001) 166–173.

[2] Y. Yang, A. Hentati, H.X. Deng, O. Dabbagh, T. Sasaki, M. Hirano, W.Y. Hung, K. Ouahchi, J. Yan, A.C. Azim, N. Cole, G. Gascon, A. Yagmour, M. Ben-Hamida, M. Pericak-Vance, F. Hentati, T. Siddique, The gene encoding alsin, a protein with three guanine-nucleotide exchange factor domains, is mutated in a form of recessive amyotrophic lateral sclerosis, Nat. Genet. 29 (2001) 160–165.

[3] J.L. Rosa, R.P. Casaroli-Marano, A.J. Buckler, S. Vilaro, M. Barbacid, p619, a giant protein related to the chromosome condensation regulator RCC1, stimulates guanine nucleotide exchange on ARF1 and Rab proteins, EMBO J. 15 (1996) 4262–4273.

[4] A. Schmidt, A. Hall, Guanine nucleotide exchange factors for Rho GTPases: turning on the switch, Genes Dev. 16 (2002) 1587–1609.

[5] D.S. Carney, B.A. Davies, B.F. Horazdovsky, Vps9 domain-containing proteins: activators of Rab5 GTPases from yeast to neurons, Trends Cell Biol. 16 (2006) 27–35.

[6] H. Takeshima, S. Komazaki, M. Nishi, M. Iino, K. Kangawa, Junctophilins: a novel family of junctional membrane complex proteins, Mol. Cell 6 (2000) 11–22.

[7] M. Zerial, H. McBride, Rab proteins as membrane organizers, Nat. Rev. Mol. Cell Biol. 2 (2001) 107–117.

[8] A. Otomo, S. Hadano, T. Okada, H. Mizumura, R. Kunita, H. Nishijima, J. Showguchi-Miyata, Y. Yanagisawa, E. Kohiki, E. Suga, M. Yasuda, H. Osuga, T. Nishimoto, S. Narumiya, J.-E. Ikeda, ALS2, a novel guanine nucleotide exchange factor for the small GTPase Rab5, is implicated in endosomal dynamics, Hum. Mol. Genet. 12 (2003) 1671–1687.

[9] R. Kunita, A. Otomo, H. Mizumura, K. Suzuki, J. Showguchi-Miyata, Y. Yanagisawa, S. Hadano, J.-E. Ikeda, Homo-oligomerization of ALS2 through its unique carboxyl-terminal regions is essential for the ALS2-associated Rab5 guanine nucleotide exchange activity and its regulatory function on endosome trafficking, J. Biol. Chem. 279 (2004) 38626–38635.

[10] J.D. Topp, N.W. Gray, R.D. Gerard, B.F. Horazdovsky, Alsin is a Rab5 and Rac1 guanine nucleotide exchange factor, J. Biol. Chem. 279 (2004) 24612–24623.

[11] K. Kanekura, Y. Hashimoto, Y. Kita, J. Sasabe, S. Aiso, I. Nishimoto, M. Matsuoka, A Rac1/phosphatidylinositol 3-kinase/Akt3 anti-apoptotic pathway, triggered by AlsinLF, the product of the ALS2 gene, antagonizes Cu/Zn-superoxide dismutase (SOD1) mutant-induced motoneuronal cell death, J. Biol. Chem. 280 (2005) 4532–4543.

[12] E.L. Tudor, M.S. Perkinton, A. Schmidt, S. Ackerley, J. Brownlees, N.J.O. Jacobsen, H.L. Byers, M. Ward, A. Hall, P.N. Leigh, C.E. Shaw, D.M. McLoughlin, C.C.J. Miller, ALS2/Alsin regulates Rac-PAK signaling and neurite outgrowth, J. Biol. Chem. 280 (2005) 34735–34740.

[13] K. Kanekura, Y. Hashimoto, T. Niikura, S. Aiso, M. Matsuoka, I. Nishimoto, Alsin, the product of ALS2 gene, suppresses SOD1 mutant neurotoxicity through RhoGEF domain by interacting with SOD1 mutants, J. Biol. Chem. 279 (2004) 19247–19256.

[14] S. Hadano, A. Otomo, K. Suzuki-Utsunomiya, R. Kunita, Y. Yanagisawa, J. Showguchi-Miyata, H. Mizumura, J.-E. Ikeda, ALS2CL, the novel protein highly homologous to the carboxy-terminal half of ALS2, binds to Rab5 and modulates endosome dynamics, FEBS Lett. 575 (2004) 64–70.

[15] S. Hadano, J.-E. Ikeda, Purification and functional analyses of ALS2 and its homologue, in: W.E. Balch, C.J. Der, A. Hall (Eds.), GTPases Regulating Membrane Targeting and Fusion, Methods in Enzymology, vol. 403, Elsevier Inc, San Diego, CA, 2005, pp. 310–321.

[16] E. Nielsen, F. Severin, J.M. Backer, A.A. Hyman, M. Zerial, Rab5 regulates motility of early endosomes on microtubules, Nat. Cell Biol. 1 (1999) 376–382.

[17] P. Pasinelli, R.H. Brown, Molecular biology of amyotrophic lateral sclerosis: insights from genetics, Nat. Rev. Neurosci. 7 (2006) 710–723.

DNA Sequence, June 2006; 17(3): 242–246

informa
healthcare

SHORT COMMUNICATION

HFM1, the human homologue of yeast Mer3, encodes a putative DNA helicase expressed specifically in germ-line cells

KAZUNORI TANAKA[1], NATSUKI MIYAMOTO[2], JUNKO SHOUGUCHI-MIYATA[1], & JOH-E IKEDA[1,2,3]

[1]*Department of Molecular Neuroscience, The Institute of Medical Sciences, Tokai University School of Medicine, Isehara, Kanagawa 259-1193, Japan,* [2]*Solution Oriented Research for Science and Technology (SORST), Japan Science and Technology Corporation, Tokai University School of Medicine, Isehara, Kanagawa 259-1193, Japan, and* [3]*Department of Paediatrics, Faculty of Medicine, University of Ottawa, Ottawa, Ontario K1H 8M5, Canada*

(Received 28 October 2005)

Abstract

DNA helicases are known to play important roles in the maintenance of genome integrity including the replication of trinucleotide repeats in the cells. Here, we report the *HFM1* gene, which encodes the putative human DNA helicase. The *HFM1* gene comprises 39 exons mapping to human chromosome 1p22.2. The *HFM1* cDNA encompasses 4931 nucleotides with a single open reading frame (ORF) of 1435 amino acid residues encoding a predicted 172 kDa protein (hHFM1). The deduced protein sequence shares similar domain and motif structures to those of Mer3, a DNA helicase of *Saccharomyces cerevisiae*; seven consecutive motifs conserved among the DEXH-box type of DNA/RNA helicases at the N-terminal and a single putative zinc finger motif at the C-terminal regions of the protein. Further, the *HFM1* transcript is preferentially expressed in testis and ovary. Collectively, hHFM1 is the evolutionally conserved putative human DNA helicase, which may function as a modulator for genome integrity in germ-line tissues.

Keywords: *HFM1, DNA helicase, Mer3, trinucleotide repeat*

Database accession number: *AB204867*

The expansions of trinucleotide repeats (TNRs), such as GCC, CGG, CTG, GAA and CAG, are known to associate with several human neurodegenerative diseases (Paulson et al. 1996). Although several models including DNA replication slippage (Freudenreich et al. 1997; Schweitzer and Livingston 1998), DNA damage repair (Kovtun and McMurray 2001) and meiotic recombination (Jankowski et al. 2000) have been proposed, the molecular mechanism by which TNR expansion occurs is still unclear. Most recently, it has been demonstrated that yeast Srs2 DNA helicase selectively unwinds TNR hairpin and blocks the expansion of TNRs (Bhattacharyya et al. 2004, 2005), suggesting a possible involvement of DNA helicases in the TNR expansion.

In this study, we sought to explore the *trans*-acting factors that associate with the instability of the TNRs in mammalian cells by the yeast one-hybrid screening system (BD Matchmaker One-Hybrid System) as described previously (Tanaka et al. 2004). Use of the genomic DNA fragment containing the TNR and its flanking DNA sequences of the human *HD* gene as a bait identified pACT2-11 cDNA (insert; ~2.2 kb in size, Genbank/EMBL/DDBJ accession number AB044787) encoding a putative DNA helicase. This human gene and its protein product have been designated as *HFM1* (HUGO Gene Nomenclature Committee) and hHFM1, respectively. Complete sequence information of the coding region for hHFM1 was achieved by 5′RACE using cDNA

Correspondence: J.-E. Ikeda, Department of Molecular Neuroscience, The Institute of Medical Sciences, Tokai University School of Medicine, Isehara, Kanagawa 259-1193, Japan. Tel: 81 463 91 5095. Fax: 81 463 91 4993. E-mail: jeikeda3@is.icc.u-tokai.ac.jp. E-mail: joh-e@mgcheo.med.uottawa.ca

ISSN 1042-5179 print/ISSN 1029-2365 online
DOI: 10.1080/10425170600805433

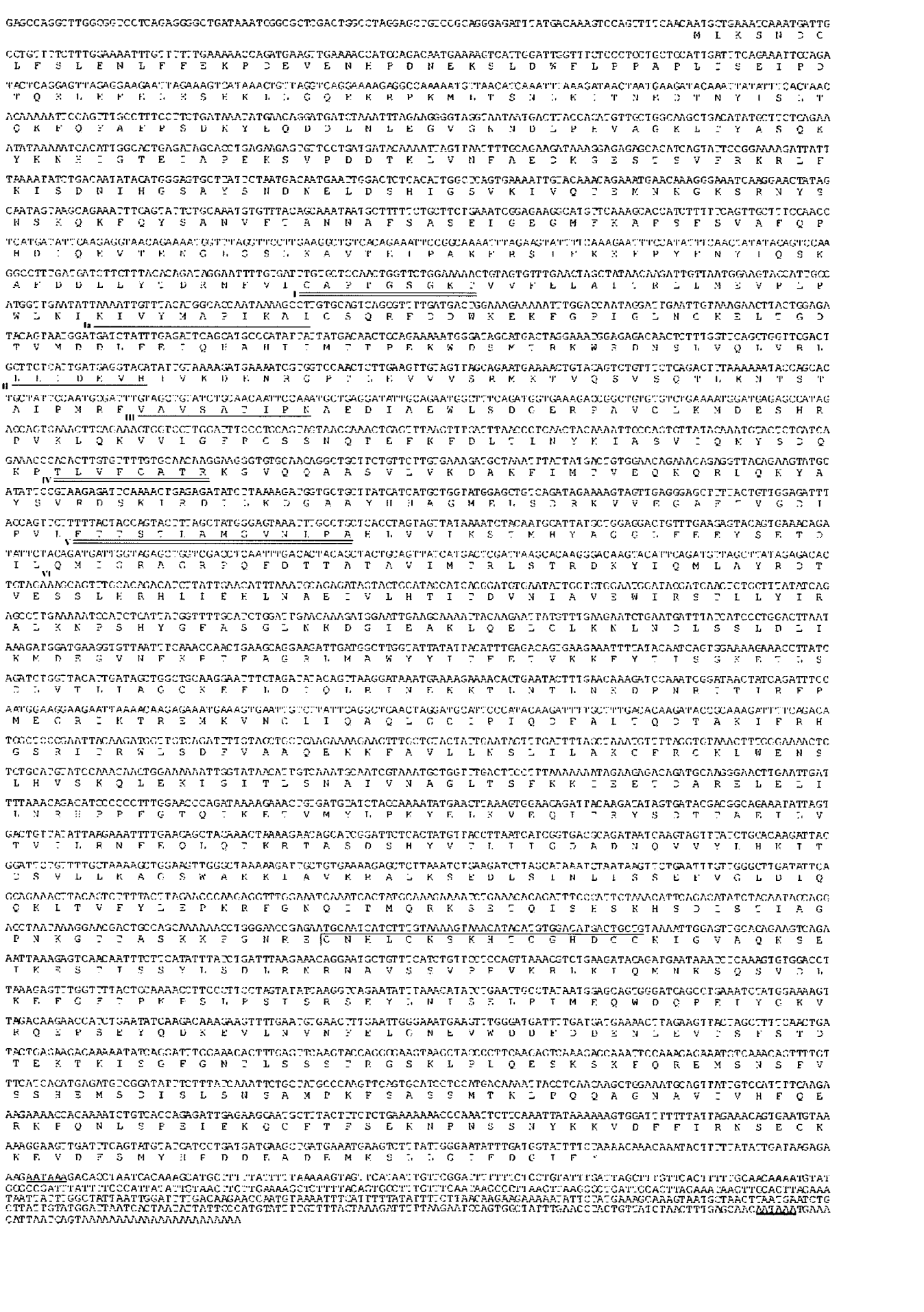

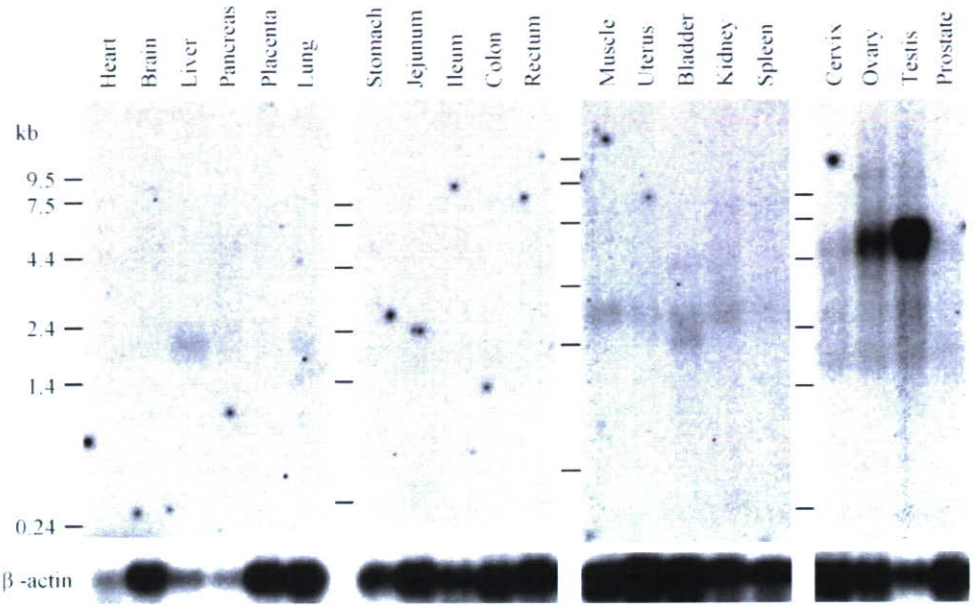

Figure 2. Northern blot analysis of the *HFM1* mRNA. Filters (Gene Hunter I, II, III and IV; non-normalized, Toyobo) were hybridized with 32p-labelled pACT2-11 cDNA or human β-actin cDNA as a probe in a solution (0.5 M sodium phosphate (pH7.2)-7% SDS-1 mM EDTA) for 18 h at 65°C. Filters were washed once for 5 min in 2 × SSC at room temperature and for another 30 min in 2 × SSC-1% SDS at 65°C. Autoradiography was performed for 5 days using X-ray film (BioMax, Kodak) at −80°C. Molecular size markers are indicated on the left.

samples from human testis. The *HFM1* cDNA of 4931 nucleotides (nt) long (pACT2-11L), comprising a single open reading frame (ORF) of 1435 amino acid residues, was obtained (Genbank/EMBL/DDBJ accession number AB204867) (Figure 1).

To define the genomic organization of the *HFM1* gene, BLAST searches of the human genome DNA sequence (Build 35, version 1) as well as non-redundant nucleotide database were conducted. This revealed that *HFM1* comprised 39 exons and resided within ~144 kb of the genomic DNA segment mapping to human chromosome 1p22.2. Further, two independent transcribed DNA sequences, which were partially overlapped with the *HFM1* cDNA sequence, have been assigned within the same genomic interval (Genbank/EMBL/DDBJ accession number AK094079; ID name FLJ36760 and NCBI GeneID 164045; Genbank/EMBL/DDBJ accession number NM_001017975 and AK096330; ID name FLJ39011) (Ota et al. 2004). Computational analyses of these cDNA sequences demonstrated that the FLJ36760 cDNA contained the DNA sequences corresponding to a part of exon 16 and entire exons from 19 to 39 with lacking exon 36 of the *HFM1* gene, while the FLJ39011 cDNA carried the sequences corresponding to a part of exon 1 and entire exons from 2 to 11 with 4nt insertion between exons 9 and 10, indicative of a cryptic splicing event, and contained a part of intron 11. It was also evident that 4nt insertion disrupted the coding frame for *HFM1*. Together, these results suggest that two previously reported cDNAs are partial and/or alternatively spliced transcribed DNA sequences for *HFM1*, and that our cDNA sequence should represent the transcript containing the full ORF (Figure 1).

To investigate the tissue distribution of the *HFM1* transcript, we performed Northern blot analysis. A major transcript of approximately 5.5 kb long was preferentially expressed in testis and ovary, while minor transcripts of approximately 1.4 kb and/or 1.6 kb were detected in liver, muscle, bladder and kidney (Figure 2). Difference in sizes between the *hHFM1* cDNA cloned and the long transcript in Northern blotting (~4.9 vs ~5.5 kb) may be due to the presence of uncloned portions of the 5′- and/or 3′-UTR for the *HFM1* mRNA sequence. Further, two minor *HFM1* transcripts observed may represent the previously-reported *HFM1* cDNA sequences (see above).

Figure 1. DNA sequence of the *HFM1* cDNA and deduced amino acid sequences of hHFM1. Seven conserved motifs (I, Ia, II, III, IV, V and VI) of DNA/RNA helicases are doubly underscored. The open box represents the putative zinc finger motif. Polyadenylation signals are underscored. The original cDNA fragment (pACT2-11) obtained by yeast one-hybrid screening encompasses the region corresponding to 2714–4954 nucleotides (nt). Primers used for 5′RACE (SMART™ RACE cDNA Amplification Kit (BD bioscience)) are as follows; 5′-GTTCCAAAGGGGGGATGTCTGTTTA-3′ (3027–3003nt), 5′-TTTACACCTAAAACATTTA-3′ (2866–2848nt), 5′-TTCTTTTCTTGAGCAGCTACA-3′ (2814–2794nt), 5′-CTTGTAATTCGGGAGCCATGTCTGA-3′ (2778–2754nt), 5′-GATGTCTGTGCAAACTGCTTTC-3′ (2186–2165nt), 5′-ACTCCCATGTATATTGTC-3′ (628–611nt), and 5′-TTTTCAACTTCATCTGG-3′ (171–155nt).

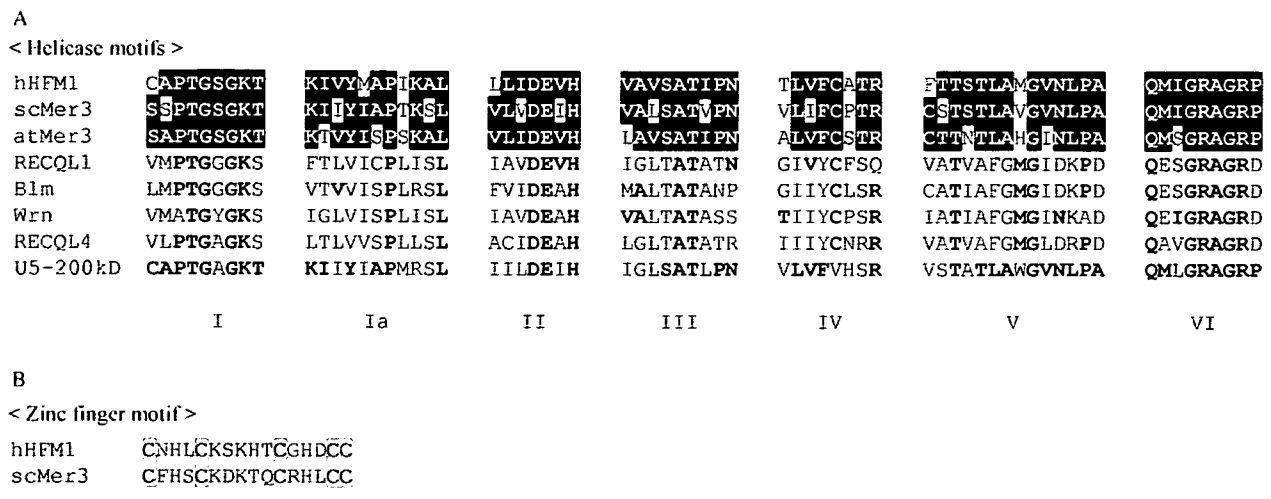

Figure 3. Multiple sequence alignment of amino acid sequences. (A) The comparison of seven consecutive motifs conserved among the DEXH-box type of DNA/RNA helicases. Amino acid residues conserved in at least two cases among hHFM1, *S. cerevisiae* Mer3 (scMer3) and *A. thaliana* Mer3 (atMer3) are marked with white letters in black boxes, and amino acid residues matched with between hHFM1 and RecQ helicase family or hHFM1 and U5-200 kDa are shown as bold. (B) Pair-wise comparison of the amino acid sequences of putative zinc finger motifs identified in hHFM1 and scMer3. Conserved cysteine residues are marked with shaded boxes.

Computational predictions have shown that a major transcript for *HFM1* encodes 172 kDa protein, termed hHFM1, consisting of 1435 amino acids (aa), and comprises several domains and motifs. In the N-terminal half of hHFM1, there are the seven consecutive motifs, which are characteristically conserved among the DEXH-box type of DNA/RNA helicases (Figure 1). These motifs are highly homologous to the helicase domains of the members of Mer3 (Nakagawa et al. 1999; Mercier et al. 2005), the members of RecQ helicase family (Opresko et al. 2004) and RNA splicing factor, U5-200 kDa (Jung et al. 2002) (Figure 3A). The high sequence similarity of seven helicase motifs between hHFM1 and known helicases suggests that hHFM1 possesses a helicase activity to unwind DNA and/or RNA. In addition, a single zinc finger motif at the C-terminal portion of hHFM1 was noted (Figure 1). All cysteine residues in the zinc finger motif were completely conserved between hHFM1 and *Saccharomyces cerevisiae* Mer3 (scMer3) (Figure 3B). Further, the overall similarity of the amino acid sequences between hHFM1 and scMer3 was significantly high with a 33% of identity (DNASIS-Mac3.5). Collectively, these data strongly suggest that hHFM1 is a human orthologue of scMer3.

In this study, we identified a putative human DNA helicase gene *HFM1*, and demonstrated that its gene product hHFM1 represented a putative mammalian homologue for scMer3. Interestingly, human HFM1 is highly expressed in germ-line tissues such as testis and ovary. As both scMer3 and its plant orthologue *Arabidopsis thaliana* Mer3 (atMer3) (Mercier et al. 2005) are known to control the formation of meiotic crossover (Nakagawa et al. 1999, 2001, 2002; Mercier et al. 2005), hHFM1 may also play a role in such physiological events particularly in germ cells.

Lastly, the recent studies of helicase and TNR expansion have revealed that yeast helicase Srs2 selectively acts on DNA substrates containing CNG repeats and prevents expansions of TNRs (Bhattacharyya et al. 2004, 2005). As we have demonstrated that hHFM1 binds preferentially to the proximal region of the CAG repeat within the *HD* gene (Tanaka et al. unpublished data), it is possible that hHFM1 also plays a role in the TNR expansion in germ cells. Further functional characterizations of hHFM1 will provide new clues to elucidate the mechanism of meiotic instability of the TNRs implicating in human neurodegenerative diseases.

Acknowledgements

We thank to Shinji Hadano for preparation of this manuscript. A part of this work has been supported by a Grant-in Aid for Scientific Research on Priority Areas-Advanced Brain Science Project-from Ministry of Education, Culture, Sports, Science and Technology, Japan.

References

Bhattacharyya S, Lahue RS. 2004. *Saccharomyces cerevisiae* Srs2 DNA helicase selectively blocks expansions of trinucleotide repeats. Mol Cell Biol 24:7324–7330.

Bhattacharyya S, Lahue RS. 2005. Srs2 helicase of *Saccharomyces cerevisiae* selectively unwinds triplet repeat DNA. J Biol Chem 280:33311–33317.

Freudenreich CH, Stavenhagen JB, Zakian VA. 1997. Stability of a CTG/CAG trinucleotide repeat in yeast is dependent on its orientation in the genome. Mol Cell Biol 17:2090–2098.

Jankowski C, Nasar F, Nag DK. 2000. Meiotic instability of CAG repeat tracts occurs by double-strand break repair in yeast. Proc Natl Acad Sci USA 97:2134–2139.

Jung D-J, Sung H-S, Goo Y-W, Lee HM, Park OK, Jung S-Y, Lim J, Kim H-J, Lee S-K, Kim TS, Lee JW, Lee YC. 2002. Novel

transcrption coactivator complex containing activating signal cointegrator 1. Mol Cell Biol 22:5203–5211.

Kovtun IV, McMurray CT. 2001. Trinucleotide expansion in haploid germ cells by gap repair. Nat Genet 27:407–411.

Mercier R, Jolivet S, Vezon D, Huppe E, Chelysheva L, Giovanni M, Nogué F, Doutriaux M-P, Horlow C, Grelon M, Mézard C. 2005. Two meiotic crossover classes cohabit in *Arabidopsis*: One is dependent on *Mer3*, whereas the other one is not. Curr Biol 15:692–701.

Nakagawa T, Kolodner RD. 2002. *Saccharomyces cerevisiae* MER3 is a DNA helicase involved in meiotic crossing over. Mol Cell Biol 22:3281–3291.

Nakagawa T, Ogawa H. 1999. The *Saccharomyces cerevisiae MER3* gene, encoding a novel helicase-like protein, is required for crossover control in meiosis. EMBO J 18:5714–5723.

Nakagawa T, Flores-Rozas H, Kolodner RD. 2001. The Mer3 helicase involved in meiotic crossing over is stimulated by single-stranded DNA-binding proteins and unwinds DNA in the 3′ to 5′ direction. J Biol Chem 276:31487–31493.

Opresko PL, Cheng W-H, Bohr VA. 2004. Junction of RecQ helicase biochemistry and human disease. J Biol Chem 279:18099–18102.

Ota T, Suzuki Y, Nishikawa T, Otsuki T, Sugiyama T, Irie R, Wakamatsu A, Hayashi K, Sato H, Nagai K, Kimura K, Makita H, Sekine M, Obayashi M, Nishi T, Shibahara T, Tanaka T, Ishii S, Yamamoto J, Saito K, Kawai Y, Isono Y, Nakamura Y, Nagahari K, Murakami K, Yasuda T, Iwayanagi T, Wagatsuma M, Shiratori A, Sudo H, Hosoiri T, Kaku Y, Kodaira H, Kondo H, Sugawara M, Takahashi M, Kanda K, Yokoi T, Furuya T, Kikkawa E, Omura Y, Abe K, Kamihara K, Katsuta N, Sato K, Tanikawa M, Yamazaki M, Ninomiya K, Ishibashi T, Yamashita H, Murakawa K, Fujimori K, Tanai H, Kimata M, Watanabe M, Hiraoka S, Chiba Y, Ishida S, Ono Y, Takiguchi S, Watanabe S, Yosida M, Hotuta T, Kusano J, Kanehori K, Takahashi-Fujii A, Hara H, Tanase TO, Nomura Y, Togiya S, Komai F, Hara R, Takeuchi K, Arita M, Imose N, Musashino K, Yuuki H, Oshima A, Sasaki N, Aotsuka S, Yoshikawa Y, Matsunawa H, Ichihara T, Shiohata N, Sano S, Moriya S, Momiyama H, Satoh N, Takami S, Terashima Y, Suzuki O, Nakagawa S, Senoh A, Mizoguchi H, Goto Y, Shimizu F, Wakebe H, Hishigaki H, Watanabe T, Sugiyama A, Takemoto M, Kawakami B, Yamazaki M, Watanabe K, Kumagai A, Itakura S, Fukuzumi Y, Fujimori Y, Komiyama M, Tashiro H, Tanigami A, Fujiwara T, Ono T, Yamada K, Fujii Y, Ozaki K, Hirao M, Ohmori Y, Kawabata A, Hikiji T, Kobatake N, Inagaki H, Ikema Y, Okamoto S, Okitani R, Kawakami T, Noguchi S, Itoh T, Shigeta K, Senba T, Matsumura K, Nakajima Y, Mizuno T, Morinaga M, Sasaki M, Togashi T, Oyama M, Hata H, Watanabe M, Komatsu T, Mizushima-Sugano J, Satoh T, Shirai Y, Takahashi Y, Nakagawa K, Okumura K, Nagase T, Nomura N, Kikuchi H, Masuho Y, Yamashita R, Nakai K, Yada T, Nakamura Y, Ohara O, Isogai T, Sugano S. 2004. Complete sequencing and characterization of 21,243 full-length human cDNAs. Nat Genet 36:40–45.

Paulson HL, Fischbeck KH. 1996. Trinucleotide repeats in neurogenetic disorders. Annu Rev Neurosci 19:79–107.

Schweitzer JK, Livingston DM. 1998. Expansions of CAG repeat tracts are frequent in a yeast mutant defective in Okazaki fragment maturation. Hum Mol Genet 7:69–74.

Tanaka K, Shouguchi-Miyata J, Miyamoto N, Ikeda J-E. 2004. Novel nuclear shuttle proteins, HDBP1 and HDP2, bind to neuronal cell-specific *cis*-regulatory element in the promoter for the human Huntington's disease gene. J Biol Chem 279:7275–7286.

MICROSCOPY RESEARCH AND TECHNIQUE 69:427–435 (2006)

Morphodynamics of Ovarian Follicles During Oogenesis in Mice

EIMEI SATO,[1]* NAOKO KIMURA,[1] MASAKI YOKOO,[1] YUKO MIYAKE,[1] AND JOH-E IKEDA[2]
[1]*Laboratory of Animal Reproduction, Graduate School of Agricultural Science, Tohoku University, Sendai 981-8555, Japan*
[2]*Department of Molecular Neuroscience, The Institute of Medical Science, Tokai University, Isehara, Japan*

KEY WORDS follicle development; atresia; oocyte; cumulus–oocyte complex; apoptosis; angiogenesis; EGF; TNF-α; glycosaminoglycans; ovary

ABSTRACT In the mouse, oogonia enter the prophase of the first meiotic division and differentiate into oocyte while developing in the fetal ovary. Shortly after birth, all oocytes are arrested in the dictyate stage of late prophase in the developing follicles; a small number of follicles reach the ovulatory stage; the rest are lost by apoptosis. The resumption of meiotic division and nuclear progression to metaphase II (oocyte maturation) occur in the ovulatory follicles. In this article we review recent morphological data that have clarified how cytokines and glycosaminoglycans (GAGs) are involved in mouse follicular development, atresia, and maturation during oogenesis, as exogenous/endogenous factors. (1) Microvascular networks and angiogenic factors (epidermal growth factor; GAGs) are deeply involved in selective mouse oocyte growth beyond ~20–30 μm in diameter. (2) Gonadotropin-inducible neuronal apoptosis inhibitory protein may indirectly affect oocyte survival as a result of the inhibition of apoptotic granulosa-cell death during folliculogenesis. (3) The pattern of oocyte degeneration depends on follicle and oocyte developmental stages, and follicle stimulating hormone accelerates the process of degeneration of oocytes. (4) The process of degeneration of mouse oocytes/eggs is modulated by tumor necrosis factor-α that is accumulated in the expanded cumulus during oocyte maturation. (5) A colloidal iron-positive substance was detected in the intercellular spaces of follicular tissue, especially in the cumulus mass. Cells located where the cumulus mass and granulosa cell layer interwound became enlarged during the resumption of oocyte meiosis. Colloidal iron-positive substances accumulated extensively within the intercellular spaces of the enlarged cells. *Microsc. Res. Tech. 69:427–435, 2006.* © 2006 Wiley-Liss, Inc.

INTRODUCTION

Most of the germ cell population rests in a pool of nongrowing small follicles in the ovary. A small percentage of oocytes and follicles starting to grow reach a certain stage of development, then degenerate or mature and ovulate. The whole process must be under both exogenous as well as endogenous control. Recent morphological works have clarified that cytokines and glycosaminoglycans (GAGs) are involved in follicular development, atresia, and maturation during oogenesis, as exogenous and endogenous factors, in mice.

Localization of Epidermal Growth Factor and GAGs in Developing Ovarian Follicles

Exogenous signals controlling the development of oocytes and follicles must be translocated in the tissue, especially via vascular networks and/or tissue fluid. When observed histologically, there is a striking difference in the distribution of blood vessels in the mammalian ovary (Macchiarelli et al., 1993). Smaller follicles possess principally circumferential vessels with few branches, while the dominant follicles are supplied with numerous polyhedral networks of vessels that project downward to the basement membrane surrounding the granulosa cells. These morphological features suggest that microvascular networks and angiogenic factors affect the oocyte and follicular growth, particularly the selective growth of oocytes and follicles. In previous studies, we demonstrated angiogenic activity of epidermal growth factor (EGF) and ovarian GAGs using an assay system in which EGF/GAG Elvax films are implanted on the lateral wall of the sheath of musculus rectus abdominis (Sato et al., 1990, 1991). We have also shown that GAGs strengthen the angiogenic activity of EGF in mice (Sato et al., 1991).

EGF is soluble in tissue fluid, can be translocated in tissues, and induces endothelial cells to proliferate and form capillaries. In the ovary, however, rapid and profound angiogenesis is restricted to a specific region (Shimoda et al., 1993).

This tissue specificity may be due to the localization of ovarian components, including GAG and EGF, to the specific region allowing angiogenesis to occur.

Ovaries of 17-day-old mouse fetuses contained clusters of oocytes less than 14.9 μm in diameter surrounded by somatic cells, not yet assembled into follicles. They were concentrated in the core of the ovary,

*Correspondence to: Eimei Sato, Laboratory of Animal Reproduction, Graduate School of Agricultural Science, Tohoku University, Aoba-ku, Sendai 981-8555, Japan. E-mail: eimei@mail.bios.tohoku.ac.jp

Received 25 October 2005; accepted in revised form 30 November 2005

Contract grant sponsor: The Japanese Society for the Promotion of Science (JSPS); Contract grant number: JSPS-RFTF 97L00904; Contract grant sponsor: Program for Promotion of Basic Research Activities for Innovative Bioscience, Brain, Japan.

DOI 10.1002/jemt.20302

Published online 22 May 2006 in Wiley InterScience (www.interscience.wiley.com).

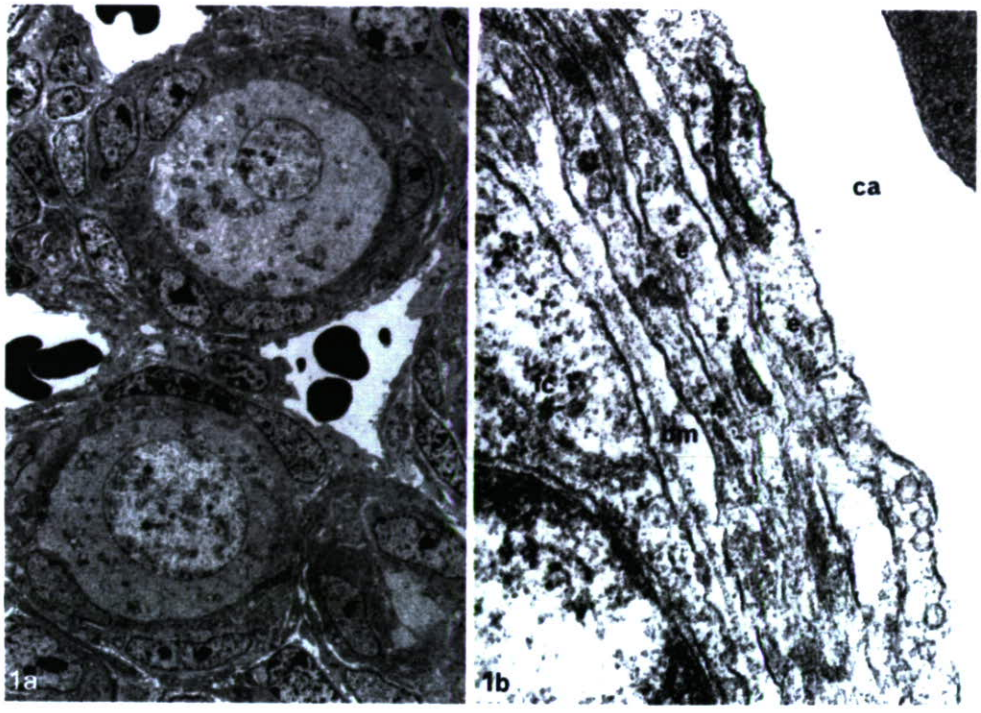

Fig. 1. Electron micrograph of the oocyte and granulosa cells in the follicle in the ovary of a 1-day-old newborn. (**a**) The follicles, including oocytes more than 20 μm in diameter, are surrounded by a capillary network. (**b**) A single layer of continuous endothelium of the capillary juxtaposed to the follicle. bm, basement membrane; fc, follicle cells; e, endothelial cells; ca, capillary; re, red blood cell.

within pocket-like structures. At birth, oocytes were surrounded by a few flat granulosa cells containing rough endoplasmic reticulum without lipid droplets and had no zona pellucida. Microvascular networks were recognized around the follicles containing oocytes more than ~20 μm in diameter (Fig. 1). The wall of capillaries juxtaposed to follicles consisted of a single layer of continuous endothelium. By day 3 after birth, distinct capillaries were observed among oocytes 30–40 μm or greater in diameter and the number of oocytes 30 μm or greater in diameter increased by day 5 after birth.

In the ovary of 3-day-old newborn mice (Fig. 2), colloidal iron-positive substances (i.e., GAGs) were observed most often around the follicles containing oocytes 30 μm or greater in diameter that had been selected to grow further (Fig. 2b, panel A). In the ovaries of 5-day-old newborns, GAGs were observed most often in the zona pellucida and the intercellular space (Fig. 2b, panels B and C). Slight staining of EGF was observed in the medulla of the ovaries of 3-day-old newborns, especially around the growing follicles (Fig. 2c, panel A). In 5-day-old newborns, distinct staining of EGF was observed in interstitial cells around growing follicles (Fig. 2c, panels B and C). In contrast, no positive EGF signal was detected in oocytes, granulosa cells, or interstitial connective tissue. There was no strict correlation between the distribution of EGF and GAGs in the ovaries of 3- or 5-day-old newborns.

As mentioned earlier, follicular growth clearly occurs in 1–5-day-old newborns. By 5 days after birth, oocytes grow in diameter from 10.0–14.9 to 45.0–49.9 μm. In our observation, follicles containing oocytes 20–30 μm in diameter came to be surrounded by apparent capillary networks, suggesting that the association of follicles with capillaries may influence the progress of growth of the oocyte. Little is known about the factors that permit some oocytes to begin and continue to grow while making others remain inert or stop growing. Histological observation suggests that follicular growth is accelerated by forming association with blood capillaries (Miyamoto et al., 1996). Numerous studies have investigated the role of EGF in the growth of ovarian follicle preovulatory development (Conti et al., 2005). EGF is produced by thecal and interstitial cells in the ovary (Carson et al., 1989). In cell culture systems, EGF was shown to enhance the proliferation of vascular endothelial cells. It also effects neovascularization in vivo (Gospodarowicz et al., 1979), and is therefore considered to be one of the major angiogenic factors in the ovary. It was demonstrated that GAGs from ovarian extracts strengthened the angiogenic activity of EGF in mice, suggesting the possibility that GAGs reinforce the induction of angiogenesis by endogenous EGF (Sato et al., 1991). During follicular growth, GAG accumulates in the follicle and outer layer of growing follicles containing oocytes more than 30 μm in diameter in the ovary of 3-day-old newborn mice. It may be that ovarian GAG interacts with EGF to induce vascularization and then accelerate the growth of oocytes in the follicles. Indeed, well developed blood vessels were identified histologically around follicles containing oocytes more than 30 μm in diameter.

Ferric chloride, when boiled with hydrazine hydrate and cacodylic acid, is converted into a fine cationic iron colloid (colloidal iron) that consists of 0.5–1.5 nm electron-dense granules and gives a distinct Prussian Blue reaction (Murakami et al., 1986). Moreover, Murakami et al. (1986) demonstrated that colloidal iron reacted with the strongly anionic particle IR-1 20 (IR-SO_3^-) at a pH range of 0.8–7.6 and with the carboxyl particle CG-50 (IR-COO^-) at a pH range of 4.0–7.6. Neither the reaction nor affinity of the colloidal iron with the cationic particle RA-400 (IR-NH_3^+) was observed in the pH range of 0.8–7.6. They also demonstrated that colloidal

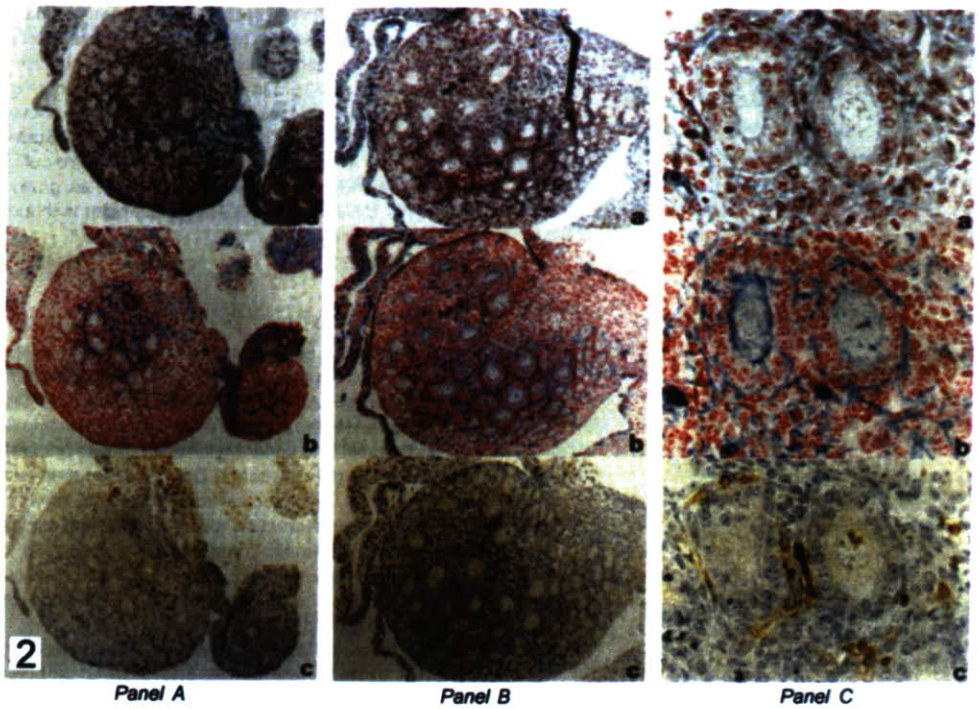

Fig. 2. Serial sections of the ovaries of (**Panel A**) 3-day-old and (**Panels B and C**) 5-day-old newborns. (**a**) Aldehyde fuchsin and Masson-Goldner's trichrome, (**b**) colloidal iron, (**c**) immunostaining of epidermal growth factor (EGF). Note the distinct staining of colloidal iron among the follicles including oocytes more than 30 μm in diameter; a slight immunoreaction of EGF is observed around the follicles including oocytes more than 30 μm in diameter (Panel A). Apparent immunoreaction of EGF is identified around the follicles including oocytes more than 40 μm in diameter (Panels B and C).

irons are more stable and that a greater staining of tissues (particularly at a low pH level) and strongly negative-charged substance, including sulfate groups, are seen at pH levels less than 4.0 (Murakami et al., 1986; Ohtsuka and Murakami, 1986). The pH value of the staining solution was adjusted to 1.8, as shown in the experiment reported in Figure 2. Therefore, colloidal iron-positive materials found extensively at the interfollicular space of growth-initiated follicles with oocytes more than 30 μm in diameter are estimated to be strongly negative-charged substances including sulfate groups.

Histochemical Detection of Neuronal Apoptosis Inhibitory Protein in the Follicles

Apoptosis is an essential process in maintaining the ovarian homeostasis in mammals (Amsterdam et al., 2003). A gene for neuronal apoptosis inhibitory protein (NAIP) has been isolated as a candidate gene for spinal muscular atrophy, which is characterized by a loss of spinal cord motor neurons, resulting in the weakening and wasting of the proximal voluntary muscles (Roy et al., 1997). This gene is a member of the inhibitor-of-apoptosis protein family of genes, which has an evolutionarily conserved role in regulating apoptotic cell death in the animal kingdom. NAIP gene expression can suppress apoptosis in several cell lines (Liston et al., 1996). Collectively, these results imply that NAIP is a novel mammalian-cell death suppressor and that it might in part be responsible for the inhibition of cell death that cannot be explained by the Bcl-2 family of proteins.

To understand the potential role of NAIP in the development of mammalian ovarian follicles, we studied its mRNA expression and hormonal regulation in mouse ovaries during neonatal, prepubertal, and pubertal development (Matsumoto et al., 1999). Mouse NAIP mRNAs were most highly expressed in the ovary from sexually mature mice at 12 and 18 week of age, when ovarian follicles consisted of primordial, primary, secondary, and antral follicles. On the other hand, low levels of expression of NAIP gene were observed in ovaries that were mostly composed of primordial follicles from neonatal 2-day-old mice and also in ovaries obtained from lactating 18-week-old mice 3 days after parturition in which follicular development was suppressed.

The expression of NAIP mRNA in the mouse ovary was evaluated by in situ hybridization with a NAIP-specific cDNA riboprobe. The sense and antisense RNAs span the coding sequence in exons 3–9 of human NAIP cDNA. This region has very high homology to the corresponding region in the mouse NAIP gene (Scharf et al., 1996). Ovaries from 2-day-old mice revealed two types of follicles: (1) primordial follicles consisting of primordial oocyte and flattened immature granulosa cells, and (2) primary follicles consisting of oocytes surrounded by one to two layers of cuboidal granulosa cells. The strong signal obtained with the antisense NAIP riboprobe was observed exclusively in the granulosa cells of primary follicles, whereas no labeled cells were detected in the primordial follicles in any of ovaries examined. In the ovaries of sexually mature mice at 12 weeks of age, both mural granulosa cells as well as cumulus cells directly surrounding the oocyte in a Graafian follicle displayed a high level of NAIP expression. Furthermore, NAIP gene expression was investigated in hypophysectomized pregnant mare serum gonadotropin (PMSG)-primed female. High NAIP gene expression was observed in granulosa cells of early antral follicles. On the other hand, the signal intensity for NAIP mRNA in some granulosa cells of preantral follicles was either absent or weak, possibly because these follicles might be undergoing atresia.

The expression of the NAIP gene in ovarian follicular cells and the role of NAIP in protecting ovarian follicu-

lar cells from apoptosis in vivo were assessed by comparison of three sequential histological sections of the mouse ovary (Fig. 3). One of these sections was examined, by TUNEL, for the nucleosomal DNA fragmentation that is characteristic of apoptotic nuclei. The other two sections were used for the analysis of NAIP mRNA expression by in situ hybridization with the antisense probe and with the sense riboprobe as a negative control, respectively. All the nonapoptotic ovarian follicles were accompanied by granulosa cells expressing a high level of NAIP mRNA (Fig. 3: left follicle). Atretic follicles, which can be identified by the presence of apoptotic granulosa cells, expressed ovarian NAIP mRNA very weakly or not at all (Fig. 3: right follicle). In addition, TUNEL-negative cells were also detected in some follicles with granulosa cells that were negative for NAIP mRNA expression. This indicates that apoptosis was not always induced in granulosa cells that did not express NAIP.

In our study, NAIP mRNA expression was shown to be restricted to granulosa cells in mouse ovarian follicles. These findings were confirmed by the RT-PCR analysis of NAIP mRNA in cultured granulosa cells. Furthermore, the apoptotic DNA breakdown is restricted to granulosa cells throughout ovarian development (Hughes and Gorospe, 1991). Together, these observations suggest that NAIP is involved in the in vivo apoptotic cascade of the ovarian follicle. The earliest signs of atresia, which are mainly observed in growing, antral, and Graafian follicles, are (1) pycnosis of nuclei of granulosa cells and (2) condensation of chromosomes in the oocyte. NAIP mRNA was nearly absent in atretic follicles. However, no apoptotic signs were observed in the ovarian follicles in which granulosa cells expressed a substantial level of NAIP mRNA. In addition, NAIP mRNA was highly expressed in the ovaries of sexually mature mice. Thus, these results suggest that NAIP might play a potential role in the survival of ovarian follicles through its antiapoptotic function. However, it is unclear why apoptosis was not observed in some granulosa cells in which NAIP was not expressed.

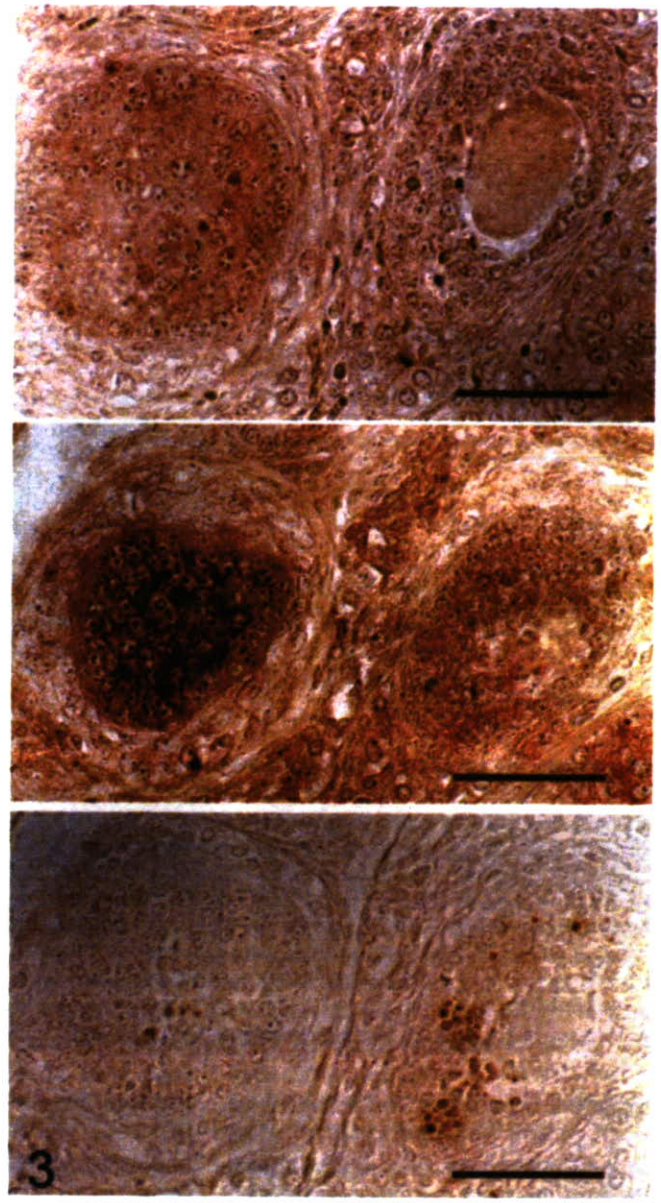

Fig. 3. In situ detection of apoptosis and mouse NAIP mRNA in granulosa cells of a nonapoptotic ovarian follicle (left) and an apoptotic follicle (right) in three sequential histological sections of the mouse ovary. Top and middle panels, analysis of NAIP mRNA expression by in situ hybridization with the sense probe (control) and the antisense probe, respectively. Bottom panel, examination of nucleosomal DNA fragmentation by TUNEL. The nonapoptotic ovarian follicle (left) is accompanied by granulosa cells expressing a high level of NAIP mRNA. Follicle with apoptotic granulosa cells (right) became atretic, with weak or no expression of NAIP mRNA in granulosa cells. Scale bars for all panels, 100 μm.

Histological Profile of Nuclear Degeneration of Oocytes in the Growing Follicles

In oocytes of atretic follicles, degeneration of nuclei and pseudomaturation division, such as germinal vesicle breakdown (GVBD), chromosomes at metaphase, or expulsion of a polar body, are observed (Fig. 4). These degenerative changes in the nucleus of oocytes are followed by fragmentation and disappearance of chromosomes. Finally, degenerated oocytes are removed from follicles by phagocytic activity of granulosa cells (Hubbard and Greenwald, 1985).

In our study, nuclear degeneration of oocytes in the follicle in stage 1 through 3 was not identified clearly under the light microscope, and it was impossible to identify the stage of development of follicles (Nakai et al., 1996) in the advanced stage of atresia.

In most type 4–7 follicles, the oocyte had a centrally located nucleus at the resting stage of the prophase. Pyknotic nuclei were absent, the zona pellucida was intact, mitotic figures were seen in the granulosa layer, and the follicular fluid was "clean," i.e. without cell debris or leukocytes. The theca interna consisted of a few concentric layers of elongated cells with a rich bed of capillaries. The total number of follicles recognized as type 4,5,6, or 7 was 335.0 ± 12.8 per ovary, and 29.0% of these follicles included oocytes with a degenerated nucleus. The percentage of follicles with a degenerated nucleus was smaller in types 6–7 than in types 4–5.

Most of the oocytes in type 4–5 follicles showed pyknosis (degenerated nuclei) or disappearance of chromosomes (on serial section examination). In type 6–7 fol-

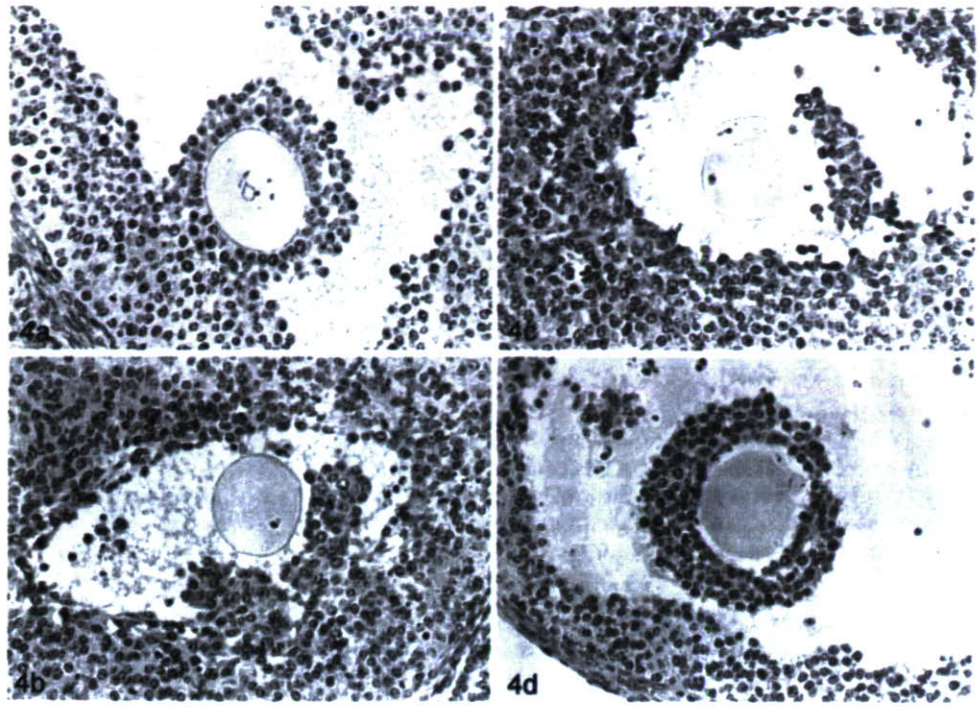

Fig. 4. Light micrographs of oocytes in vesicular follicles of 32–34-day-old mouse ovary (×80). (**a**) The oocyte with germinal vesicle; (**b**)–(**c**) The oocytes showing resumption of meiosis. The chromosomes with spindles at the first (b) and second (c) metaphase are observed at the surface of oocytes. First polar body is evident (c and d). The cumulus oophorus has undergone extensive degeneration (b and c). The cumulus–oocyte complex is detached from granulosa cell layer (d).

licles, pseudomaturation division (progression to diakinesis, metaphase I and II, anaphase I), activation, and pycnotic changes were observed. The dominant stage of the pseudomaturation division was metaphase I or II. About 3% of oocytes did not possess chromosomes, as shown by serial section examination.

To clarify the relationship between oocyte size and degenerative changes, degenerating oocytes in type 4–7 follicles were classified according to the diameter of the oocytes. Most of the oocytes ranging from 61 to 70 μm in diameter showed pseudomaturation in metaphase I or II and anaphase I. The number of oocytes with pyknotic changes (i.e., condensation of chromosomes) was small. Very few oocytes (3.5%) were activated and possessed pronucleus-like structures. None of the oocytes with a diameter less than 50 μm had meiosis-like changes such as presence of chromosomes in metaphase or polar body. Pyknotic changes and the disappearance of chromosomes were dominant in oocytes with a diameter less than 60 μm. Taken together, among the oocytes measuring more than 51 μm in diameter in type 6–7 follicles, degenerating oocytes showed pseudomaturation division. In type 4–5 follicles, pyknotic changes (condensation of chromosomes) and disappearance of chromosomes were dominant.

The administration of follicle stimulating hormone (FSH) did not increase the total number of type 4–5 follicles, but increased the number of type 6–7 follicles. The number of oocytes with a degenerating nucleus decreases significantly after the administration of FSH in types 4–6 and 6–7 follicles. These observations are in agreement with those in rats (Braw and Tsafriri, 1980). Moreover, FSH significantly decreased the number of follicles containing degenerating oocytes. An antiatretic effect of PMSG on the large mouse follicles has been reported (Peters, 1979). It was inferred that the surge of FSH rescues the type 5 follicles from atresia, thus allowing them to reach ovulation in the next cycle (Tsafriri and Braw, 1984). Tsafriri and Braw (1984) demonstrated an effect of PMSG in rescuing immature rat follicles of type 5 and 6 from atresia. Estrogen treatment prevents follicular atresia in hypophysectomized immature female rats (Daud et al., 1988), and it is possible that FSH and PMSG exert their antiatretic action through the stimulation of follicular estrogen production.

The induction of superovulation with PMSG in mice is a well-established and widely used procedure. Whether this effect of PMSG results from recruitment of follicles from the nongrowing pool or from a decrease in the rate of atresia is apparently specific to the species. In immature mice, administration of PMSG decreased the number of large atretic follicles and therefore it has been suggested that gonadotropin prevents the atretic process (Peters, 1979). On the other hand, in the ovary of the cyclic hamster PMSG not only decreases follicular atresia but also recruits "reserve" follicles (Chiras and Greenwald, 1978). However, the morphological features of the action of FSH/PMSG on follicular recruitment and atresia are still under investigation.

A small fraction of the FSH binding was seen on atretic follicles while the overwhelming majority of FSH-binding at all stages of the estrous cycle was seen on healthy follicles (Byskov, 1974). Byskov (1974) suggested that PMSG induces the granulosa cells of atretic follicles to phagocytose the dying cells and thus rescues the follicles at an early stage of atresia. If FSH/PMSG rescues the type 4–5 follicles, including degenerating oocytes, and stimulates the development of follicles, the number of type 6–7 follicles with degenerating oocytes should increase. In our study, however, we clarify that the number of type 4–5 and 6–7 follicles with degenerating oocytes after FSH administration was smaller than that of the control. We reported that FSH/

PMSG does not stimulate the development of atretic follicles. It is therefore possible that FSH fastens the degeneration of atretic follicles. It is also speculated that cytokines produced by macrophages influence the phagocytotic activity of granulosa cells to remove degenerating oocytes.

Macrophages were identified in the interstitial tissue, especially around the follicles. The intensity of immunostaining of the macrophage was greatly reduced when the antimacrophage monoclonal antibody was replaced by normal mouse ascites. Strong positive staining and a large number of macrophages were observed around the follicles with degenerating oocytes. It was reported that macrophages accumulate in perifollicular sites during follicular development and demise of Graafian follicles (Nakai et al., 1996; Sato et al., 1995b). One of the cytokines produced by macrophages, the tumor necrosis factor-α (TNF-α), is present in the mouse ovary (Carswell et al., 1975). In our study, a significant immunostaining of TNF-α was identified in oocytes of atretic follicles. Oocytes showing positive immunostaining of TNF-α had some characteristics of degeneration (Carswell et al., 1975). TNF-α has been shown to participate in the regulation of cellular growth (Pennica et al., 1985) and exerts potent necrotic effects on transplantable tumors in vivo (Palladino et al., 1987). Strong immunoreaction for TNF-α was detected in the shrunken oocytes in the atretic follicles, suggesting that TNF-α was expressed during the degenerative process and/or accumulated inside the shrunken oocytes (Carswell et al., 1975). In our study, a number of macrophages were observed around the follicles with degenerating oocytes, suggesting the possibility that macrophages secrete TNF-α, which binds to oocytes to stimulate the process of degeneration.

Immunohistochemical Detection of TNF-α in Graafian Follicles and Its Possible Physiological Roles

In the ovary, lymphocytes, macrophages, mast cells, and other lymphopoietic cells are present in perifollicular, paraluteal, and intraluteal sites at various times during the development and demise of Graafian follicles (Bagavandoss et al., 1988). TNF-α and TNF-α mRNA is also present in the rat ovary (Roby and Terranova, 1989). These observations have led to the hypothesis that TNF-α affects the oocytes situated in the follicles. In the course of our investigation on oocyte maturation, the immunohistochemical localization of TNF-α in the ovary was determined and the effects of TNF-α and anti-TNF-α antiserum on the maturation and degeneration of oocytes were examined in vitro (Sato et al., 1993). A strong signal stained with anti-TNF-α antibody was detected in the expanded cumulus. The most intensive signal was observed in the expanded cumulus in the Graafian follicles at 6 h after human chorionic gonadotropin (hCG) administration (Fig. 5). Normal rabbit serum gave no specific signals in the expanded cumulus.

TNF-α did not influence GVBD or the formation of the first polar body at concentrations of 1 or 10 ng/mL. Cultured oocytes were examined every 24 h for fragmentation. The earliest fragmented oocyte was detected 48 h after culture. At 72 and 120 h of culture, about 40 and 75% of cumulus-free oocytes, respectively,

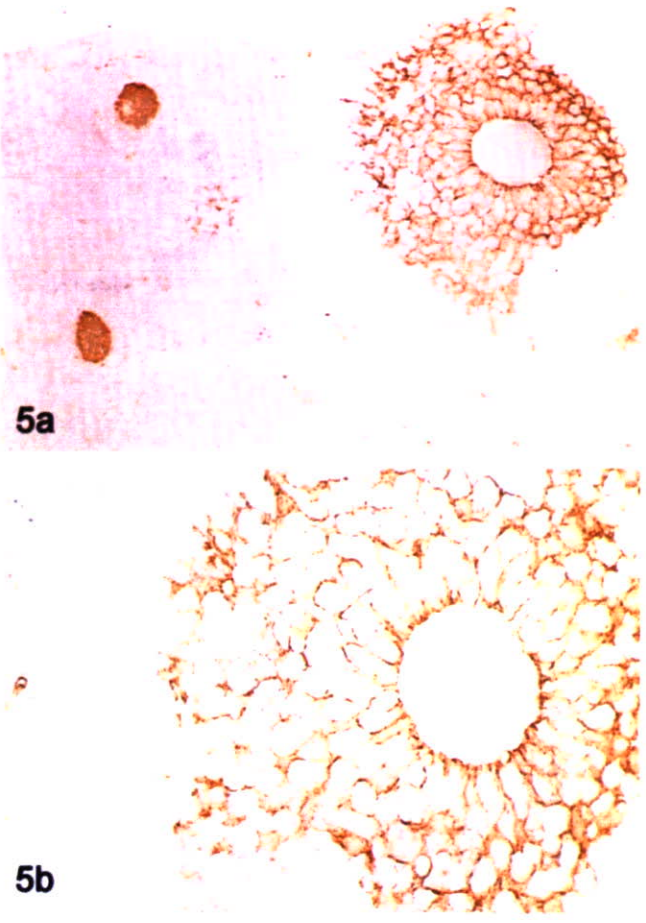

Fig. 5. Imunohistochemical detection of TNF-α protein in a section of mouse ovary. Staining of mouse ovary by anti-TNF-α antiserum. Ovaries removed at 6 h after hCG administration. Cumulus cells surrounding the oocyte that had induced GVBD in the Graafian follicle were stained very intensely. The corona radiata and cumulus mass became dispersed, showing the typical morphology of a maturing cumulus oocyte complex. TNF-α was also observed in the oocytes in the atretic follicles. (a) ×100; (b) ×200.

had undergone spontaneous fragmentation. The fragmented oocyte consisted of numerous blastomeres of various sizes. Ghost-like blastomeres were also identified in the space among fragmented blastomeres (Fig. 6). At concentrations of 1 and 10 ng/mL, TNF-α suppressed the occurrence of spontaneous fragmentation of cultured cumulus-free mouse oocytes. The incidence of fragmented oocytes decreased with increasing concentrations of TNF-α in the medium when examined 120 h after in vitro culture. The effect of TNF-α on the spontaneous fragmentation of cumulus-free oviductal oocytes was also examined in the culture. At 1 and 10 ng/mL, TNF-α did not suppress fragmentation.

In cumulus-free oocytes the sensitivity between follicular and oviductal oocytes to TNF-α is different. Likely, the hyaluronidase treatment performed during the preparation causes the loss of sensitivity of oviduct cumulus-free oocytes to TNF-α.

There were no significant differences in the percentages of oocytes undergoing GVBD or in the formation of the first polar body between the control oocytes and the oocytes incubated with anti-TNF-α antiserum, but

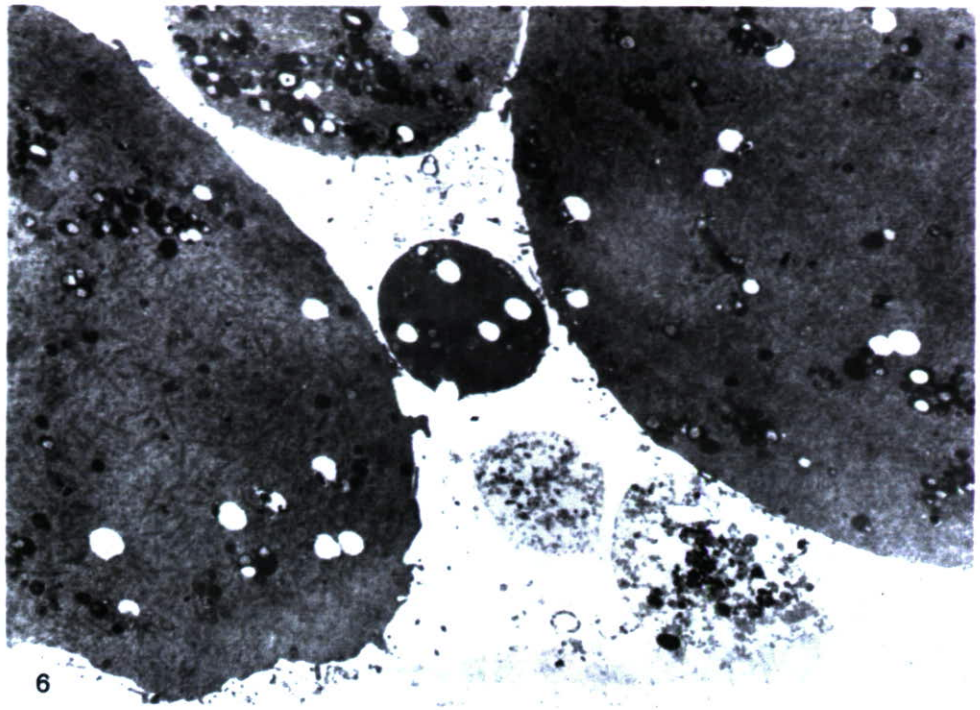

Fig. 6. Electron microphotograph of fragmented mouse oocytes cultured for 48 h in vitro. Note the presence of numerous ghost-like blastomeres among fragmented blastomeres (×8,000).

spontaneous fragmentation of follicular oocytes was accelerated in the presence of anti-TNF-α antiserum. Cultured cumulus-enclosed follicular oocytes were examined every 24 h for fragmentation. The earliest fragmented oocyte was detected 72 h after culture. At 72 and 120 h of culture, about 25 and 58% of cumulus-enclosed oocytes, respectively, had undergone spontaneous fragmentation. The percentage of cumulus-enclosed oocytes showing fragmentation was significantly lower ($P < 0.05$) than that of cumulus-free oocytes with fragmentation at 72, 96, and 120 h of culture.

The intercellular matrix of the expanded cumulus contains abundant GAGs, and the expansion of the cumulus is quite positively correlated with the production of the GAGs-hyaluronic acid by the cumulus–oocyte complex (Ball et al., 1982).

Immunohistochemical localization of TNF-α partially coincides with the distribution of GAGs, suggesting that TNF-α is associated with the intercellular GAGs of cumulus cells. We have demonstrated that the preparations of ovarian GAGs, and hyaluronic acid and chondroitin sulfate from a commercial source prevented the occurrence of fragmentation (Sato et al., 1987). GAG might interact with TNF-α to strength fragmentation-inhibitory activity. Since TNF-α has been shown to arrest cell growth, it is possible that cumulus TNF-α may participate in the suppression of the induction of fragmentation of oocytes. In our study. TNF-α suppressed spontaneous fragmentation of mouse follicular oocytes, and anti-TNF-α antiserum stimulated the induction of fragmentation of follicular cumulus-enclosed oocytes, although TNF-α and anti-TNF-α antiserum had no effect on spontaneous GVBD or polar body extrusion. Most of the cumulus cells surrounding the oocyte dispersed and disappeared within 14 h after ovulation (Sato et al., 1995a), and fragmentation is induced in cumulus-free unfertilized oocytes at 96 h after ovulation in vivo. In an in vitro culture system, the presence of attached cumulus cells prevented the spontaneous fragmentation of isolated oocytes (Sato et al., 1987). These observations might indicate that cumulus cells have a protective role against fragmentation. In this study, TNF-α was found in the cytoplasm of cumulus cells surrounding the maturing oocytes, and suppressed the spontaneous fragmentation of oocytes in vitro, suggesting that TNF-α is one of the factors produced by cumulus cells that may prevent fragmentation of oocytes.

Morphodynamics of Cumulus–Oocyte Complexes During Oocyte Maturation

In the Graafian follicles, following the preovulatory surge of gonadotropin, there is an expansion of the cumulus complex owing to the production of GAGs by the follicular tissue (Ball et al., 1982). These observations indicate that the GAGs formed within the follicles may be involved in the resumption of the meiosis of oocytes. Therefore, we tried to reveal the chronological changes of mouse cumulus–oocyte complexes and the distribution of GAGs in follicular tissue after the administration of PMSG and hCG (Sato et al., 1993; Yokoo and Sato, 2004).

All oocytes in normal Graafian follicles contained an intact germinal vesicle (GV) for 2 h after hCG injection. The GV underwent dissolution 3 h after hCG stimulation. Nine hours after hCG injection, about 20% of oocytes progressed to metaphase II. A majority of the oocytes extruded the first polar body 11 h after hCG stimulation. A dense cumulus cell mass and oocyte with an intact GV were found in the follicles in ovaries isolated 48 h after PMSG injection (0 h after hCG injection). The cumulus–oocyte complex became prominent after hCG administration, and the number of cumulus cells associated with the granulosa cell layer decreased

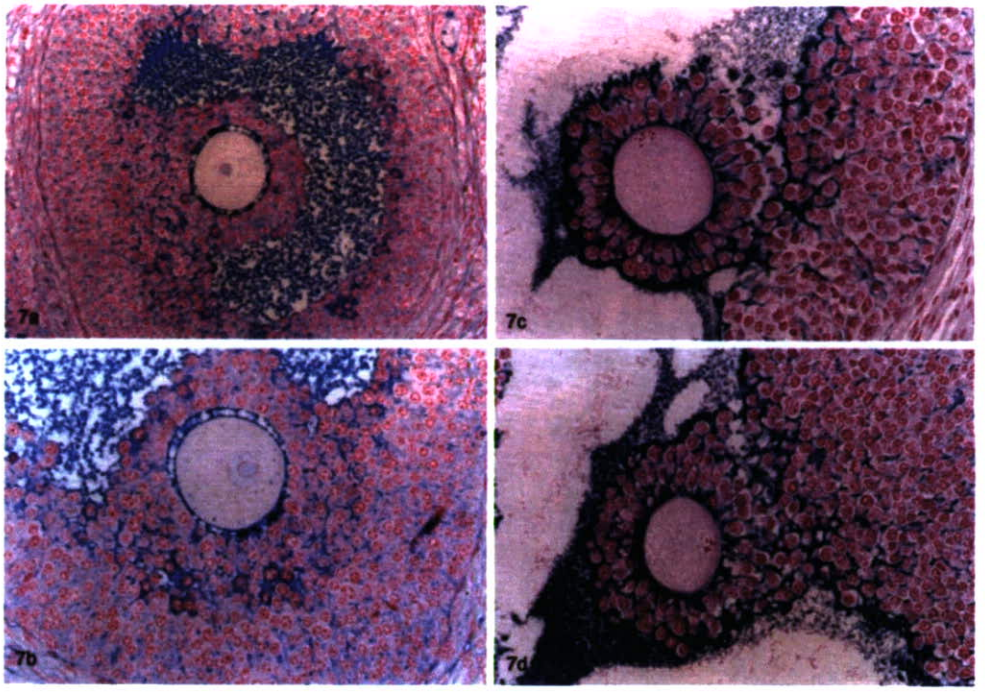

Fig. 7. Distribution of colloidal iron-positive substance (blue) in the Graafian follicular tissue at 0 (**a**), 1 (**b**), and 3 (**c** and **d**) h after hCG administration. Note the presence of enlarged cells where the cumulus mass and granulosa cell layers interwound and the extensive accumulation of colloidal iron-positive substances in the spaces between the enlarged cells (c and d). (a) ×150; (b)–(d) ×200.

significantly 1 h after hCG injection. Expansion of the cumulus cell investment was observed in the complexes in the Graafian follicles with maturing oocytes 3 h after hCG injection. Subsequently, the cumulus became less compact. Histological examination of ovaries in mice injected with PMSG and hCG revealed that GVBD was induced over 3 h after hCG administration. There is a time lag in the induction of GVBD in oocytes between in vivo and in vitro conditions, its cause being unknown. The cumulus–oocyte complex containing matured oocytes consists of dispersed cumulus cells. These findings suggest that the resumption of meiosis and the dispersion of the cumulus cell mass are interrelated during the oocyte maturation process in the mouse.

The majority of the cumulus cells associated with oocytes were round in shape, loosely arranged, and possessed prominent round or oval nuclei in those cumulus–oocyte complexes obtained from mice just after hCG stimulation. Three hours after hCG administration, the cumulus cell became dispersed as a result of the deposition of intercellular materials. Contacts between cumulus cells were reduced. The cumulus cells became dispersed because of extensive deposition of materials in the intercellular spaces. The dispersion of cells occurred during meiotic maturation not only in the cumulus–oocyte complexes but also in the granulosa cell layer. However, the degree of dispersion was greater in the cumulus mass than in the granulosa cell layer.

The cumulus–oocyte complexes and granulosa cells of the mouse ovaries after staining with colloidal irons are shown in Figure 7. Materials that were deposited in the intercellular space of cumulus cells in Graafian follicles in ovaries obtained from mice 48 h after PMSG injection were stained with colloidal iron (Fig. 7a). One hour after hCG administration, colloidal iron-positive materials were clearly visible at the peripheral area of the cumulus cell mass (Fig. 7b). After 3 h of hCG administration, a partial expansion of the cumulus cell investment and granulosa cell layer was observed in the complexes, especially those with GVBD-induced oocytes. Furthermore, the cells located at the connection site of the cumulus–oocyte complex and granulosa cell layer became enlarged, and colloidal iron-positive substances occupied the intercellular spaces between these enlarged cells and at the inner part of the cumulus mass (Figs. 7c and 7d).

Resumption of meiosis of cumulus-enclosed oocytes can be prevented by their being associated with the granulosa cell layer (Sato et al., 1982). The meiosis-arresting activity of the granulosa cells is demonstrable only when they adhere to the cumulus–oocyte complex (Sato et al., 1982). On the basis of these studies, a substance with meiosis-arresting activity from the intercellular matrix and the external surfaces of granulosa cells has been isolated (Sato and Koide, 1987) and designated as the granulosa cell factor (GCF). Moreover, we have demonstrated that GAGs interact with GCF and nullify its meiosis-arresting activity (Sato and Koide, 1987). As shown in this article, GAGs were detected extensively within the intercellular spaces of the cells between the cumulus mass and granulosa cell layer prior to the resumption of the meiosis of oocytes. These observations suggest that GAGs accumulated between the cumulus mass and granulosa cell layer interrupt the flow of GCF from granulosa cells to the oocyte, protect them from the arresting influence of GCF, and induce the resumption of meiosis of oocytes. We have demonstrated that colloidal iron-positive materials are found extensively at the intercellular space of the cumulus mass, especially at the site of the intertwining of the cumulus oophorus and granulosa cell layer. Chondroitin is the major GAG associated with proteoglycans isolated from the follicular fluid

(Grimek et al., 1984) or secreted by rat granulosa cells in vitro (Yanagishita and Hascall, 1983). Heparan sulfate was also identified in the follicular fluid (Grimek and Ax, 1982). Hyaluronic acid is the GAG produced during mucification accompanying the expansion of the cumuli in the mouse (Chen et al., 1993). These findings suggest that colloidal iron-positive materials in mouse ovarian follicles may be chondroitin, heparan sulfate, and hyaluronic acid. Molecular species of the GAGs occurring at the specific region of the follicles remain to be identified.

ACKNOWLEDGMENTS

We duly acknowledge the work and contributions from several postdoctoral associates in our group as well as external colleagues.

REFERENCES

Amsterdam A, Keren-Tal I, Aharoni D, Dantes A, Land-Bracha A, Rimon E, Sasson R, Hirsh L. 2003. Steroidogenesis and apoptosis in the mammalian ovary. Steroids 68:861–867.

Bagavandoss P, Kunkel SL, Wiggins RC, Keyes PL. 1988. Tumor necrosis factor-α (TNF-α) production and localization of macrophages and T lymphocytes in the rabbit corpus luteum. Endocrinology 122:1185–1187.

Ball GD, Bellin ME, Ax RL, First NL. 1982. Glycosaminoglycans in bovine cumulus-oocyte complexes: morphology and chemistry. Mol Cell Endocrinol 28:113–122.

Braw RH, Tsafriri A. 1980. Effect of PMSG on follicular atresia in the immature rat ovary. J Reprod Fertil 59:267–272.

Byskov AGS. 1974. Cell kinetic studies of follicle atresia in the mouse ovary. J Reprod Fertil 37:277–285.

Carson RS, Zhang Z, Hutchinson LA, Herington AC, Findlay JF. 1989. Growth factors in ovarian function. J Reprod Fertil 85:735–746.

Carswell EA, Old LK, Kassel RL, Green S, Fiore N, Williamson B. 1975. An endotoxin-induced serum factor that causes necrosis of tumors. Proc Natl Acad Sci USA 72:3666–3670.

Chen L, Russell L, Larsen WJ. 1993. Functional significance of cumulus expansion in the mouse: roles for the preovulatory synthesis of hyaluronic acid within the cumulus mass. Mol Reprod Dev 34:87–93.

Chiras DD, Greenwald GS. 1978. Effects of steroids and gonadotropins on follicular development in the hypophysectomized hamster. Am J Anat 152:307–319.

Conti M, Hsieh M, Park JY, Su YQ. Jul 28, 2006. Role of the EGF network in ovarian follicles. Mol Endocrinol (in press).

Daud AI, Bumpus FM, Husain A. 1988. Evidence for selective expression of angiotensin II receptors on atretic follicles in the rat ovary: an autoradiographic study. Endocrinology 122:2727–2734.

Gospodarowicz D, Bialecki H, Thakral TK. 1979. The angiogenic activity of the fibroblast and epidermal growth factor. Exp Eye Res 28:501–514.

Grimek HJ, Ax RL. 1982. Chromatographic comparison of chondroitin-containing proteoglycan from small and large bovine ovarian follicles. Biochem Biophys Res Commun 104:1402–1406.

Grimek HJ, Bellin ME, Ax RL. 1984. Characteristics of proteoglycans isolated from small and large bovine ovarian follicles. Biol Reprod 30:397–409.

Hubbard CJ, Greenwald GS. 1985. Morphological changes in atretic Graafian follicles during induced atresia in the hamster. Anat Rec 212:353–357.

Hughes FM, Gorospe WC. 1991. Biochemical identification of apoptosis (programmed cell death) in granulosa cells: evidence for a potential mechanism underlying follicular atresia. Endocrinology 129: 2415–2422.

Liston P, Roy N, Tamai K, Lefebvre C, Baird S, Cherton-Horvat G, Farahani R, McLean M, Ikeda J-E, MacKenzie A, Korneluk RG. 1996. Suppression of apoptosis in mammalian cells by NAIP and a related family of IAP genes. Nature 379:349–353.

Macchiarelli G, Nottola SA, Vizza E, Familiari G, Murakami T, Motta PM. 1993. Microvasculature of growing and atretic follicles in the rabbit ovary: a SEM study of corrosion casts. Arch Histol Cytol 56: 1–12.

Matsumoto K, Nakayama T, Sakai H, Tanemura K, Osuga H, Sato E, Ikeda J. 1999. Neuronal apoptosis inhibitory protein (NAIP) may enhance the survival of granulosa cells thus indirectly affecting oocyte survival. Mol Reprod Dev 54:103–111.

Miyamoto Y, Nakayama T, Haraguchi S, Miyamoto H, Sato E. 1996. Morphological evaluation of microvascular networks and angiogenic factors in the selective growth of oocytes and follicles in the ovaries of mouse fetuses and newborns. Dev Growth Differ 38:291–298.

Murakami T, Taguchi T, Ohtsuka A. 1986. A modified method of fine-granular cationic iron colloid preparation: its use in light and electron microscopic detection of anionic sites in the rat kidney glomerulus and certain other tissues. Arch Histol Jpn 49:13–23.

Nakai T, Miyamoto Y, Nakayama T, Manabe N, Sato E. 1996. Histological profiles of nuclear degeneration of oocytes in mouse ovaries and possible roles of follicle stimulating hormone for nuclear degeneration of oocytes in the atretic follicles. J Mamm Ova Res 13:24–29.

Ohtsuka A, Murakami T. 1986. Fine anionic iron colloid and its use in light and electron microscopic detection of cationic sites in the rat kidney. Arch Histol Jpn 49:543–552.

Palladino MA, Jr, Shalaby MR, Kramer SM, Ferraiolo BL, Baughman RA, Delco AB, Crase D, Marafino B, Aggarwal BB, Figari IS. 1987. Characterization of the antitumor activities of human tumor necrosis factor-α and the comparison with other cytokines: induction of tumor specific immunity. J Immunol 138:4023–4032.

Pennica D, Hayflick JS, Bringman TS, Palladino MA, Goeddel DV. 1985. Cloning and expression *Escherichia coli* of the cDNA for murine tumor necrosis factor. Proc Natl Acad Sci USA 82:6060–6064.

Peters H. 1979. Some aspects of early follicular development. In: Midgley AR, Jr, Sadler WA, editors. Ovarian follicular development and function. New York: Raven Press. pp. 1–13.

Roby KF, Terranova PF. 1988. Tumor necrosis factor-α alters follicular steroidgenesis in vitro. Endocrinology 123:2952–2954.

Roy N, Deveraux QL, Takahashi R, Salvesen GS, Reed JC. 1997. The c-IAP-1 and c-IAP-2 proteins are direct inhibitors of specific caspases. EMBO J 16:6914–6925.

Sato E, Koide SS. 1987. Biochemical transmitters regulating the arrest and resumption of meiosis in oocytes. Int Rev Cytol 106:1–33.

Sato E, Ishibashi T, Iritani A. 1982. Meiotic arresting substance separated from porcine ovarian granulosa cells and hypothetical arresting mechanism of meiosis. In: Channing CP, Segal SJ, editors. Intraovarian control mechanisms. New York: Plenum. pp. 161–173.

Sato E, Ishibashi T, Koide SS. 1987. Prevention of spontaneous degeneration of mouse oocytes in culture by ovarian glycosaminoglycans. Biol Reprod 37:371–376.

Sato E, Miyamoto H, Koide SS. 1990. Hyaluronic acid-like substance from mouse ovaries with angiogenic activity. Z Naturforsch C 45: 873–880.

Sato E, Tanaka T, Takeya T, Miyamoto H, Koide SS. 1991. Ovarian glycosaminoglycans potentiate angiogenic activity of epidermal growth factor in mice. Endocrinology 128:2402–2406.

Sato E, Inoue M, Toyoda Y. 1993. Morphological profiles of mouse ovarian follicles: extensive accumulation of a strongly negative-charged substance at specific foci in follicular tissue during oocyte maturation. Arch Histol Cytol 56:293–302.

Sato E, Ando N, Takahashi Y, Miyamoto H, Toyoda Y. 1995a. Structural changes in the oviductal wall during the passage of unfertilized cumulus-oocyte complexes in mice. Anat Rec 241:363–368.

Sato E, Nakayama T, Kamio K, Takahashi Y, Toyoda Y. 1995b. Immunohistochemical localization and possible physiological roles of tumor necrosis factor-α in mouse cumulus-oocyte complexes. Dev Growth Differ 37:413–420.

Scharf JM, Damron D, Frisella A, Bruno S, Beggs AH, Kunkel LM, Dietrich WF. 1996. The mouse region syntenic for human spinal muscular atrophy lies within the Lgn I critical interval and contains multiple copies of NAIP exon 5. Genomics 38:405–417.

Shimoda K, Sato E, Tanaka T, Takeya T, Toyoda Y. 1993. Morphological differentiation of the microvasculature during follicular development, ovulation and luteinization of mouse ovaries. Dev Growth Differ 35:431–437.

Tsafriri A, Braw RH. 1984. Experimental approaches to atresia in mammals. Oxf Rev Reprod Biol 6:226–265.

Yanagishita M, Hascall VC. 1983. Characterization of low buoyant density dermatansulfate proteoglycans synthesized by rat ovarian granulosa cells in culture. J Biol Chem 258:12847–12856.

Yokoo M, Sato E. 2004. Cumulus-oocyte complex interactions during oocyte maturation. Int Rev Cytol 235:251–291.